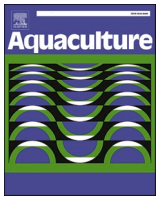
Aquaculture 625 (2026) 744287



Contents lists available at ScienceDirect

Aquaculture

journal homepage: www.elsevier.com/locate/aquaculture





Gill remodelling in Hefang bream during hypoxia and reoxygenation: Histological and transcriptomic insights

Xinxin Yu [a,b,1], Minghui Xiao [a,b,1], Siyu Fan [a,b], Zhifeng Zhou [a,b], Zhong Tang [a,b], Ming Wen [a,b], Shengnan Li [a,b], Yuequn Wang [a,b], Min Tao [a,b,*], Shaojun Liu [a,b,*]

[a] *Engineering Research Center of Polyploid Fish Reproduction and Breeding of the State Education Ministry, College of Life Sciences, Hunan Normal University, Changsha 410081, Hunan, China*

[b] *Yuelushan Laboratory, Changsha 410128, China*

ARTICLE INFO

Keywords:
Hefang bream
Hypoxic stress
Gill morphological remodelling
Transcriptome

ABSTRACT

The Hefang bream (HFB) was developed through two rounds of backcrossing after hybridization between blunt snout bream (*Megalobrama amblycephala*) and topmouth culter (*Culter alburnus*). This study focuses on the gill remodelling process in HFB under hypoxic conditions. Three experimental groups were established: a normoxic control group (HFB-D0), a 48-h hypoxia stress group (HFB-D48), and a 24-h reoxygenation group (HFB-R24). The mechanism of gill remodelling under hypoxia and reoxygenation was explored through transcriptomic and histological analyses. HE staining results showed that hypoxic stress caused damage to the gill tissue structure, which gradually returned to normal after reoxygenation. A total of 3160 differentially expressed genes (DEGs) were identified between HFB-D0 vs HFB-D48. Meanwhile, 2399 DEGs were identified between HFB-D48 vs HFB-R24. During the hypoxic phase, upstream signalling pathways associated with proliferation, including the MAPK, Wnt, Notch, TGF-β, and Hedgehog pathways, were significantly activated. The core downstream pathways involved in proliferation, namely the cell cycle and DNA replication, were also activated during hypoxia. After reoxygenation, the proliferation-related pathways returned to normal levels. IF results showed that the relative integrated fluorescence signal of HFB-D48 group was about 6.4 times that of HFB-D0 group ($P < 0.05$). The cytoskeleton-related pathway in muscle cells was activated during the hypoxic phase, whereas it was down-regulated during reoxygenation. Mucosal barrier factors (*IL-17a/f1*, *IL-22*) were reduced ($P < 0.05$) during both hypoxia and reoxygenation. An immune response centered around chemokines (*cxcl8a*, *cxcl12a*) was formed during the reoxygenation phase. The ribosome pathway was significantly upregulated after reoxygenation. PPI analysis revealed that in the comparison of HFB-D0 vs HFB-D48, the hub genes were *cdk1*, *aurka*, *plk1*, and *birc5a*. In the comparison of HFB-D48 vs HFB-R24, the hub genes were *col1a1a*, *col4a1*, *col1a2*, and *col6a1*. In conclusion, HFB gill tissue undergoes stage specific cell proliferation during hypoxia to repair damage. During reoxygenation, the focus turned to structural remodelling and immune regulation to restore homeostasis.

1. Introduction

Dissolved oxygen is a critical environmental factor in aquatic ecosystems, directly affecting the survival, growth, and distribution of aquatic organisms (Xiao, 2015). In recent years, global climate change, eutrophication of water bodies, and intensification of aquaculture have exerted multiple pressures. These pressures have led to an exacerbation of the water hypoxia phenomenon. Consequently, it has evolved into a global environmental issue that poses a threat to the protection of fishery resources and the sustainable development of aquaculture (Wu, 2002). Therefore, an in-depth study of the adaptation mechanisms of fish to hypoxia stress holds significant ecological importance for assessing ecosystem health. It also provides a theoretical basis for breeding aquaculture varieties with enhanced stress resistance. To adapt to hypoxic environments, fish have developed a series of complex adaptive strategies throughout evolution, ranging from behavioral and

* Corresponding authors at: Engineering Research Center of Polyploid Fish Reproduction and Breeding of the State Education Ministry, College of Life Sciences, Hunan Normal University, Changsha 410081, Hunan, China.
E-mail addresses: minmindiu@126.com (M. Tao), lsj@hunnu.edu.cn (S. Liu).
[1] These authors contributed equally to the study.

https://doi.org/10.1016/j.aquaculture.2026.744287
Received 12 March 2026; Received in revised form 14 May 2026; Accepted 2 June 2026
Available online 6 June 2026
0044-8486/© 2026 Published by Elsevier B.V.

Table 1
Primers used in this experiment for quantitative RT-PCR.

Genes	Forward (5′-3′)	Reverse (5′-3′)
18S	ACCGCAGCTAGGAATAATGG	GGTCGGAACTACGACGGTAT
pdgfbb	ACCACACAACGGACAGGAAC	GAGAAGGGCTCTCATTGCAG
wnt5b	ACTGGAAACGCAAGCTCCAA	GTGAAGAGCCTCCTTTGTTTGC
notch1a	CCCGGATACACAGGCTCAAT	GGTTGCTGGAACACTCGTTG
dhh	CTGCTGACTGCGGGTCTTTA	AGTCCTTACAGCGCTTGGTC
fstb	AGGCTCCTGCAACTCACTCT	GGAGTCCTGCTGTTGAAGGT
cdk1	GACATACAACATCCGCACGC	ACCACACCATACGTACCTTCAC
cdc6	CGTAAACGCACGGGTGATGA	GAAGACCGGTGTGTTCTCGT
mrps14	TCGAGGTCAGTGCTGGATCA	GACTTCTGCAGGCCTGTCTAC
rps29	TCCCGATCGAGAGAGACGAG	GAGCAAACTCGGCAGGATCT
mcm7	GATCTACGGTCACGAGGACG	AGTGGTGTACTGACTGCGAG
pold1	ACCTCTCAGGATGTTTGCTGC	TCCTCCCACTCTGTGCTCAT
itga1	CGGAGATGTCTACAGGTGCC	GAGGACCACAGGCCAGAAAC
col6a1	CCCTCCTTCAGAGAGTGTCC	GCATGTCTTGCAGCTCATCG
thbs4b	ACATGGATGGAGATGGGGTG	CACGATCCAGCTGATCACGA
itgb3b	GATGCTGGACTAGGCTCCAA	CACCAGGCACAGGTAGGATG
bcl2a	GAGGAAAATGGAGGTTGGACCTT	GACAGATGCCCTAACCCAGG
casp3b	TAGGATTGGAAACCGCGCC	CTGTCCGACATGGTCAAGGTG
serpine1	CTTGCACCGCTTTGGAGGAT	TATACTGAGGCTCTGCATTCTGAAA
ccnb1	GCTTTGAGGAAGAAGGAGGTGA	GCCTGACACAGATCATCCGA
irf7	TCGATAAACCCCTCCCACCT	GGTTTGCCGATTGTGCTCTG
stat1b	ATCAGCCCGAAAGTCTGCTC	TTGCGATGGATTCCCAGTCA
il17a/f1	CGTACCTAAACCACTGCGGA	CATACAAGCCACCACGAGGA
cxcl8a	TGGAGCTCTACCCTCCTAGC	CACGGTGCTTTGTTGGCAAG
crfb2	CCCATTCGTGGCACTACGTT	ACCACACAGAGCGAACGATT
nfkbiab	CCGAAGACGGAGACACGTTTT	GATGACGGCCAAATGCAAGG

Note: *pdgfbb*: Platelet-derived growth factor beta polypeptide (or subunit B); *wnt5b*: Wnt family member 5b; *notch1a*: Notch receptor 1a; *dhh*: Desert hedgehog signalling molecule; *fstb*: Follistatin b; *cdk1*: Cyclin-dependent kinase 1; *cdc6*: Cell division cycle 6; *mcm7*: Minichromosome maintenance complex component 7; *pold1*: DNA polymerase delta 1, catalytic subunit; *ccnb1*: Cyclin B1; *bcl2a*: B-cell CLL/lymphoma 2a; *casp3b*: Caspase 3b, apoptosis-related cysteine peptidase; *mrps14*: Mitochondrial ribosomal protein S14; *rps29*: Ribosomal protein S29; *itga1*: Integrin subunit alpha 1; *itgb3b*: Integrin subunit beta 3b; *col6a1*: Collagen type VI alpha 1 chain; *thbs4b*: Thrombospondin 4b; *irf7*: Interferon regulatory factor 7; *stat1b*: Signal transducer and activator of transcription 1b; *il17a/f1*: Interleukin 17A/F 1; *cxcl8a*: C-X-C motif chemokine ligand 8a; *crfb2*: Cytokine receptor family member b2; *nfkbiab*: NF-kappa-B inhibitor alpha b; *serpine1*: Serpin family E member 1.

physiological to molecular levels (Bickler and Buck, 2007; Nilsson et al., 2012; Nilsson and Renshaw, 2004; Stecyk et al., 2004; Zhu et al., 2013). At the physiological level, common adaptive strategies include lowering the critical oxygen tension, suppressing metabolic rates, and increasing the oxygen affinity of hemoglobin (Roesner et al., 2008). At the organ level, the gills are the primary organs responsible for gas exchange, ion regulation, acid-base balance, and nitrogenous waste excretion. It exhibits structural plasticity (i.e., gill remodelling). This is considered one of the key adaptive mechanisms for fish to cope with hypoxia stress (Nilsson, 2007; Nilsson et al., 2012). This process is typically characterized by an increase in the surface area of gill lamellae and a reduction in the volume of interlamellar cell mass, thereby enhancing oxygen uptake efficiency (Dhillon et al., 2013). However, gill remodelling also has a dual nature: while it enhances gas exchange capacity, it may also increase the risk of pathogen invasion (Nilsson, 2007). Currently, most research focuses on the static description of gill morphology or the exploration of single signalling pathways (such as the HIF pathway) (Semenza, 2010; Weidemann and Johnson, 2008). However, the temporal dynamics of this adaptive remodelling and the underlying gene regulatory programmes at the systems level remain poorly understood. A key challenge is to link gill structural changes to the cellular and molecular networks that drive them, which is essential for elucidating the mechanisms of hypoxia adaptation in fish.

Gill remodelling under hypoxic conditions is not merely a morphological adjustment but also involves complex cellular and molecular responses. Previous studies have shown that changes in gill morphology are associated with apoptosis (Shuang et al., 2022), cell proliferation (Sales et al., 2017) and cell adhesion (Liu et al., 2024). These processes can alter lamellar morphology, epithelial thickness, and respiratory surface area, thereby affecting gas exchange capacity during hypoxic stress and subsequent reoxygenation. Grass carp undergo gill remodelling in response to hypoxic environments, characterized by a reduction in interlamellar cell mass and an increase in respiratory surface area. Grass carp undergo gill remodelling in response to hypoxic environments, characterized by a reduction in interlamellar cell mass and an increase in respiratory surface area (Xu et al., 2022). Gill mucous cells and mitochondria-rich cells play important roles in hypoxia-induced gill remodelling in largemouth bass and are regulated by integrins (Liu et al., 2024). Hypoxia and reoxygenation not only affect gill morphology but also induce oxidative stress and immune responses in the gills. Hypoxia stress damages silver carp gill tissue and triggers a marked immune response by activating immune-related pathways, including complement and coagulation cascades, NOD-like receptor signalling, and Th1/Th2 cell differentiation, with differential expression of immune genes such as *cd45*, and *cd40* (Li et al., 2022). After 2 h of hypoxia exposure in *Oreochromis niloticus*, gill antioxidant enzyme activities decreased, whereas malondialdehyde content increased (Tao et al., 2024). Hypoxia stress in *Oreochromis niloticus* gills up-regulates innate immune responses while suppressing adaptive immunity, with immune-related pathways such as natural killer cell-mediated cytotoxicity and primary immunodeficiency significantly enriched (Ma et al., 2023).

The Hefang bream (*Megalobrama amblycephala* × *Culter alburnus*, HFB) is a novel hybrid bream species developed through distant hybridization between the female blunt snout bream (*Megalobrama amblycephala*, BSB) and the male topmouth culter (*Culter alburnus*, TC), followed by two rounds of backcrossing (Bundgaard et al., 2020; Gong et al., 2021; Ren et al., 2019). Our research group previous genetic characterization showed that this hybrid bream was generated through two rounds of backcrossing and possessed 48 chromosomes (Gong et al., 2021). Analyses of genetic composition showed that the 5S rDNA and *HoxD10a* sequences of HFB were inherited from the two genomes of the original parental species, BSB and TC. In addition, HFB possessed higher muscle protein levels and lower muscle carbohydrate levels than BSB. This species is an important freshwater economic fish in China, and

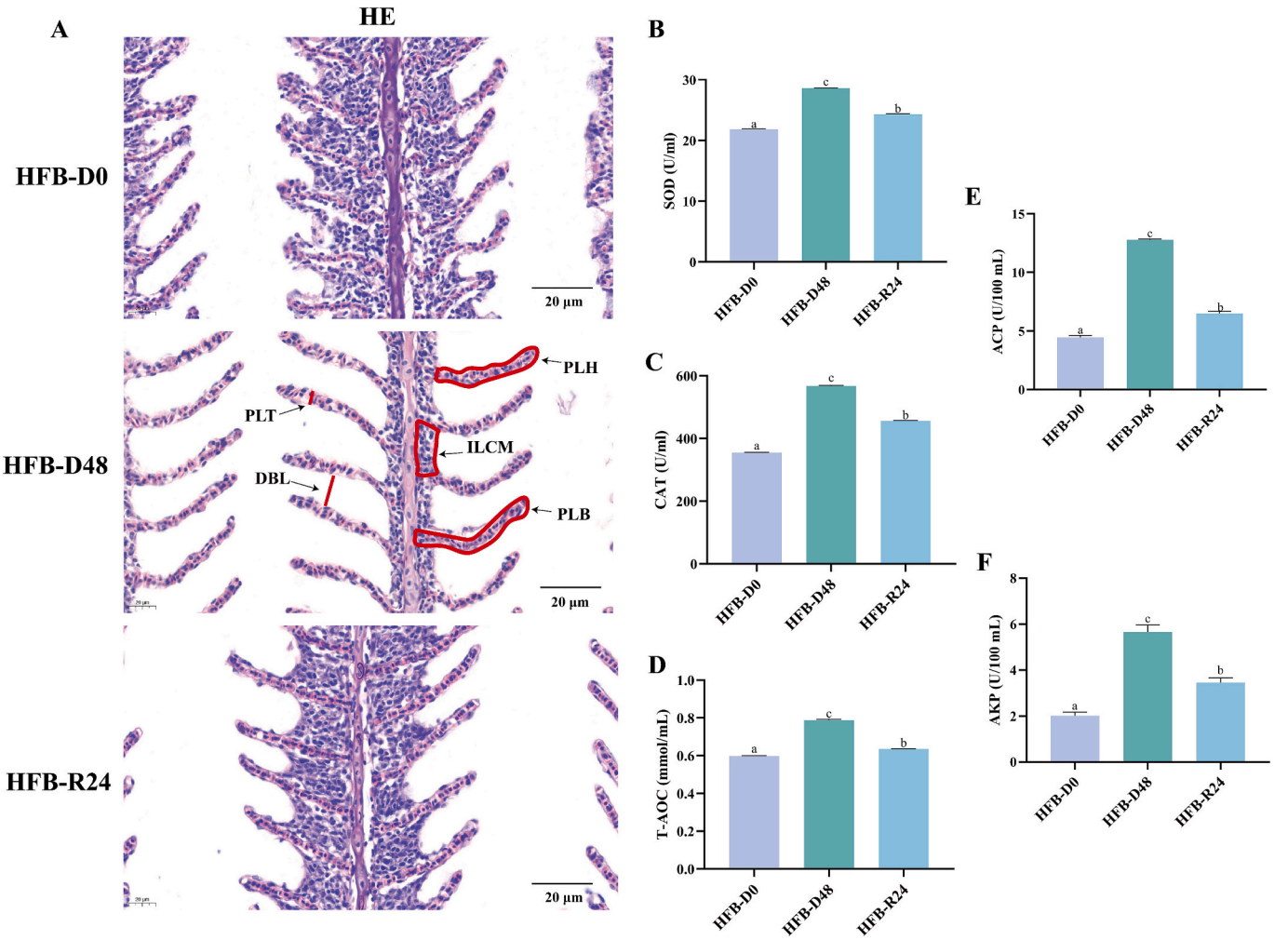


Fig. 1. Hefang bream gill histology and enzyme activity analysis. A: H&E-stained gill sections; B–D: Antioxidant enzyme activity in gill tissue; E–F: Immune enzyme activity in gill tissue. Data are presented as mean ± SEM, $n = 3$. Different lowercase letters indicate significant differences among groups based on one-way ANOVA followed by Duncan's multiple range test ($P < 0.05$). PLH: Protruding lamella height; PLB: Protruding lamella basal length; PLT: Protruding lamella thickness; DBL: Distance between lamellae; ILCM: interlamellar cell mass.

preliminary studies have shown that it possesses strong tolerance to hypoxia (Wen et al., 2025), making it an ideal model for hypoxia tolerance research. High-throughput sequencing technology enables a comprehensive characterization of dynamic changes in gene expression during hypoxic exposure. This approach enables the identification of key genes and signalling pathways, facilitating the generation of rich datasets on transcriptional responses to low-oxygen environments. These datasets, in turn, delineate stage-specific features of gene regulation across different phases of hypoxia. This study used the hypoxia-tolerant HFB as a model. Transcriptome sequencing and histopathological observations were integrated to systematically investigate the morphological and molecular responses associated with gill remodelling at representative stages of hypoxic stress and reoxygenation. These findings provide a theoretical framework for understanding the regulatory mechanisms underlying gill plasticity in fish.

2. Materials and methods

2.1. Fish rearing

The experimental fish used in this study were purchased from Chengyi Aquaculture Co., Ltd. in Guangzhou. The fish were bred in April 2025 and reared in the same pond until they reached the 6-month post-hatch stage. All fish were derived from the same breeding batch of HFB offspring (derived from three males and three females). The experimental fish (weighing 25–30 g) were kept in 100-l glass tanks in the laboratory. During a 14-day acclimation period, water quality parameters were kept stable: dissolved oxygen was maintained at 7–8.0 mg/L, water temperature was kept at 24.3 ± 0.5 °C, and pH was maintained at 7.5 ± 0.1.

2.2. Hypoxic stress and sample collection

The hypoxic stress experiment was conducted in glass tanks (100*L*), each filled with pre-aerated water, with other conditions kept consistent with the acclimation period. Three groups were established: the normoxic group (dissolved oxygen 7.0 ± 0.2 mg/L, HFB-D0), the hypoxic group (dissolved oxygen 2.0 ± 0.2 mg/L, HFB-D48), and the reoxygenation group (dissolved oxygen 7.0 ± 0.2 mg/L, HFB-R24). The hypoxia concentration used in this study was determined based on the results of preliminary experiments and the oxygen concentrations commonly used in studies of hypoxia in fish (Dagoudo et al., 2021; Halina and Sokolova, 2023; Wu et al., 2020). This design was intended to induce a clear hypoxic challenge while maintaining fish survival and avoiding severe loss of equilibrium or mortality, thereby facilitating the evaluation of early recovery responses after reoxygenation. The normoxic group was continuously aerated, while the hypoxic group had the dissolved oxygen level adjusted by introducing nitrogen gas. Dissolved oxygen was

Table 2
Effects of hypoxic on the gill morphological characteristics of HFB.

Item	Gill morphometry (24.3 °C, DO of hypoxia was kept at 2.0 mg/L)		
	0 h	48 h	R24 h
PLH (μm)	34.00 ± 2.19[a]	87.47 ± 1.91[c]	40.86 ± 0.93[b]
PLB (μm)	87.19 ± 1.66[b]	97.77 ± 2.10[c]	84.60 ± 0.39[a]
PLT (μm)	14.53 ± 0.29[c]	6.49 ± 0.38[a]	9.71 ± 0.46[b]
DBL (μm)	27.27 ± 0.96[a]	28.10 ± 1.12[a]	27.27 ± 0.88[a]
ILCM height (μm)	42.78 ± 3.69[c]	11.53 ± 0.42[a]	38.71 ± 0.46[b]
Lamellar surface area (10^4 μm^2)	0.69 ± 0.03[a]	3.03 ± 0.10[c]	0.90 ± 0.03[b]
ILCM (10^4 μm^3)	10.39 ± 1.11[c]	3.18 ± 0.19[a]	8.88 ± 0.40[b]
Water-blood diffusion distance (μm)	9.30 ± 1.07[c]	2.87 ± 0.62[a]	4.99 ± 1.62[b]

Note: ILCM = interlamellar cell mass. Data are presented as mean ± SEM, n = 3. Different lowercase letters indicate significant differences among groups based on one-way ANOVA followed by Duncan's multiple range test ($P < 0.05$). PLH: Protruding lamella height; PLB: Protruding lamella basal length; PLT: Protruding lamella thickness; DBL: Distance between lamellae; ILCM: interlamellar cell mass;

monitored every 2 h using a dissolved oxygen meter. Each group included 3 parallel replicates, with 30 experimental fish per replicate.

Gill tissue from the normoxic group fish was collected as the control group, labeled as D0. The fish were euthanized rapidly using MS 222 (50 mg/L) and dissected on ice. The second piece of gill tissue on the left side was stored in 4% paraformaldehyde for HE staining, and fluorescence immunohistochemical experiments. The remaining left gill was used for enzyme activity detection. The right gill was stored at −80 °C for transcriptome sequencing and qPCR experiments. After collecting the normoxic samples, nitrogen gas was continuously supplied to the glass tank to reduce the dissolved oxygen concentration to 2.0 mg/L. The gill tissues of the hypoxic group were collected after 48 h of hypoxic stress, labeled as D48, using the same collection method. After collecting the hypoxic samples, oxygen gas was continuously supplied to the glass tank, restoring the dissolved oxygen concentration to 7.0 mg/L. The gill tissues were collected 24 h after reoxygenation, labeled as R24, using the same collection method. At each sampling time point, three fish were randomly selected as independent biological replicates for enzyme activity assays, transcriptome sequencing, and qPCR analysis. The animal protocol utilized in this study was approved by the Ethics Committee of Hunan Normal University.

2.3. Gill tissue enzyme activity measurement

Activities of antioxidant and immunological enzymes in gill tissues, including superoxide dismutase (SOD, A001-3-2), catalase (CAT, A007-1-1), total antioxidant capacity (T-AOC, A015-3-1), acid phosphatase (ACP, A060-2-2), and alkaline phosphatase (AKP, A059-2-2), were determined using commercial kits. All assays were performed in strict accordance with the manufacturer's instructions (Nanjing Jiancheng Biological Engineering Institute, China).

2.4. Tissue sectioning and gill filament morphological measurement

After fixation in 4% paraformaldehyde for 48 h, tissues were

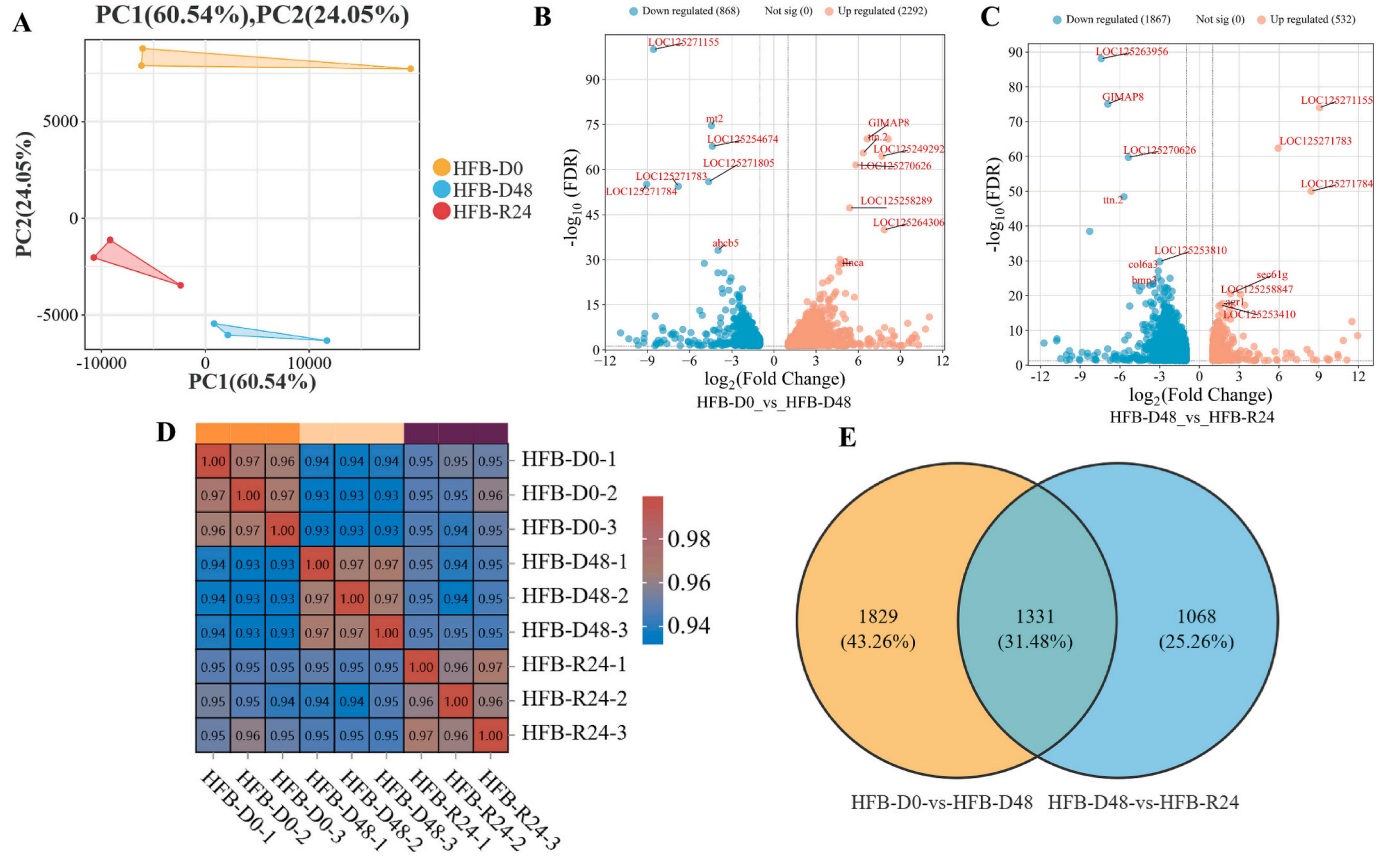


Fig. 2. Basic Analysis of Transcriptome Differences. A: Principal component analysis (PCA) of all samples. B–C: Volcano plots of differentially expressed genes (DEGs) for each comparison. D: Sample-to-sample correlation heatmap. E: Venn diagram of shared and unique DEGs among comparisons. Transcriptomic data were analyzed using the Omicsmart online platform. Differentially expressed genes were identified according to the screening criteria described in the methods section.

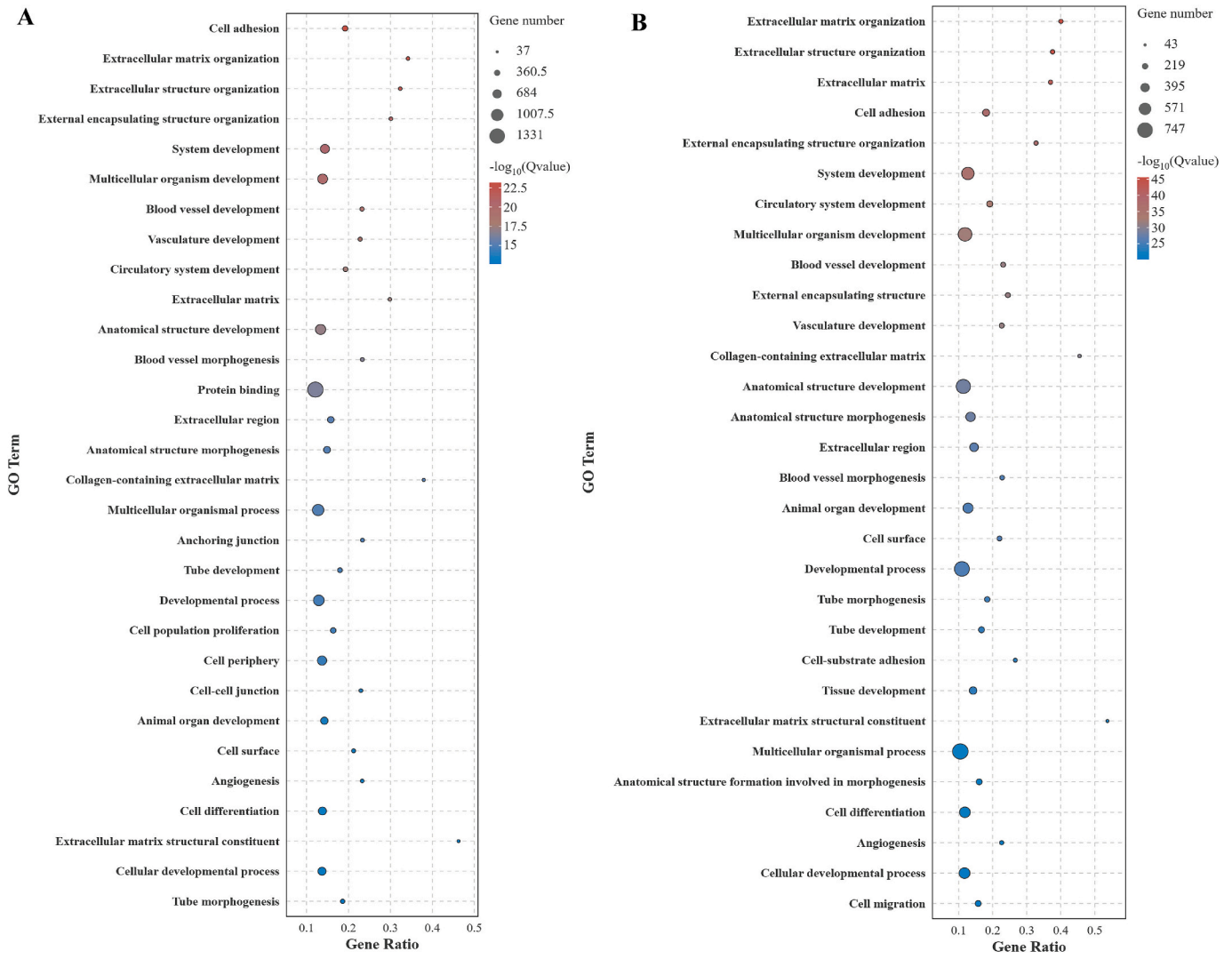


Fig. 3. GO enrichment analyses. A: GO terms enriched in DEGs for HFB-D0 vs HFB-D48. B: GO terms enriched in DEGs for HFB-D48 vs HFB-R24. Transcriptomic data were analyzed using the Omicsmart online platform. Differentially expressed genes were identified according to the screening criteria described in the methods section.

dehydrated through a graded ethanol series, embedded in paraffin, and sectioned at a thickness of 7 μm; twelve consecutive sections were collected from each sample. Routine hematoxylin-eosin (H&E) staining was performed for histological examination. Following H&E staining, morphological differences were examined and photographed. Morphometric parameters were quantified using ImageJ (https://imagej.net/software/imagej/), including: (1) Protruding lamella height (PLH); (2) Protruding lamella thickness (PLT); (3) Protruding lamella basal length (PLB); (4) Distance between lamellae (DBL); and (5) interlamellar cell mass (ILCM). The main components of the water-blood diffusion distance include the lamellar epithelial cells, basement membrane and flange region of pillar cells. The measurement and calculation of the above indicators were performed according to previously described methods (Sollid et al., 2003; Yu et al., 2023). Parameter (1)–(3) were used to estimate the respiratory surface area of the gill secondary lamellae, and parameters (3)–(5) were used to estimate ILCM volume. A total of 30 morphometric measurements were obtained from the three biological replicates at each time point for each gill structural parameter. The calculation of gill lamellar surface area and ILCM volume was performed according to the method described by Matey et al. (2008). The corresponding calculation methods are as follows:

(1) the basal length of the protruding gill lamella (l); (2) the thickness of the gill lamella (t); (3) the distance between two adjacent gill lamellae (d); (4) the height of the protruding gill lamella (h); (5) the height of the interlamellar cell mass (H). (6) gill lamellar surface area (a: μm^2); (7) the ellipse circumference formula divided by 2 (p: μm); (8) ILCM volume (V: μm^3);

$$①a = pl;\ ②p = \frac{2\pi\sqrt{\frac{1}{2}\left(r^2 + h^2\right)}}{2};\ ③r = \frac{t}{2};\ ④V = dHl.$$

2.5. Immunofluorescence (IF)

Sampling and sectioning were performed as described for HE staining. After dewaxing and rehydration, the sections were rinsed in distilled water for 1 min, three times. They were then transferred to a water bath for antigen retrieval using the commercial reagent (C1051, baipiandu, China) at 100 °C for 15 min. After cooling to room temperature, the slides were washed three times with PBS, and any residual buffer was carefully removed. The sample area on the slides was outlined using an immunohistochemistry pen (GT1001, Gene Tech, China), and autofluorescence quenching reagent (C1040, baipiandu, China) was added to the outlined area for 5 min, followed by washing with running water for 10 min. BSA (C5001, baipiandu, China) was added and incubated for 30

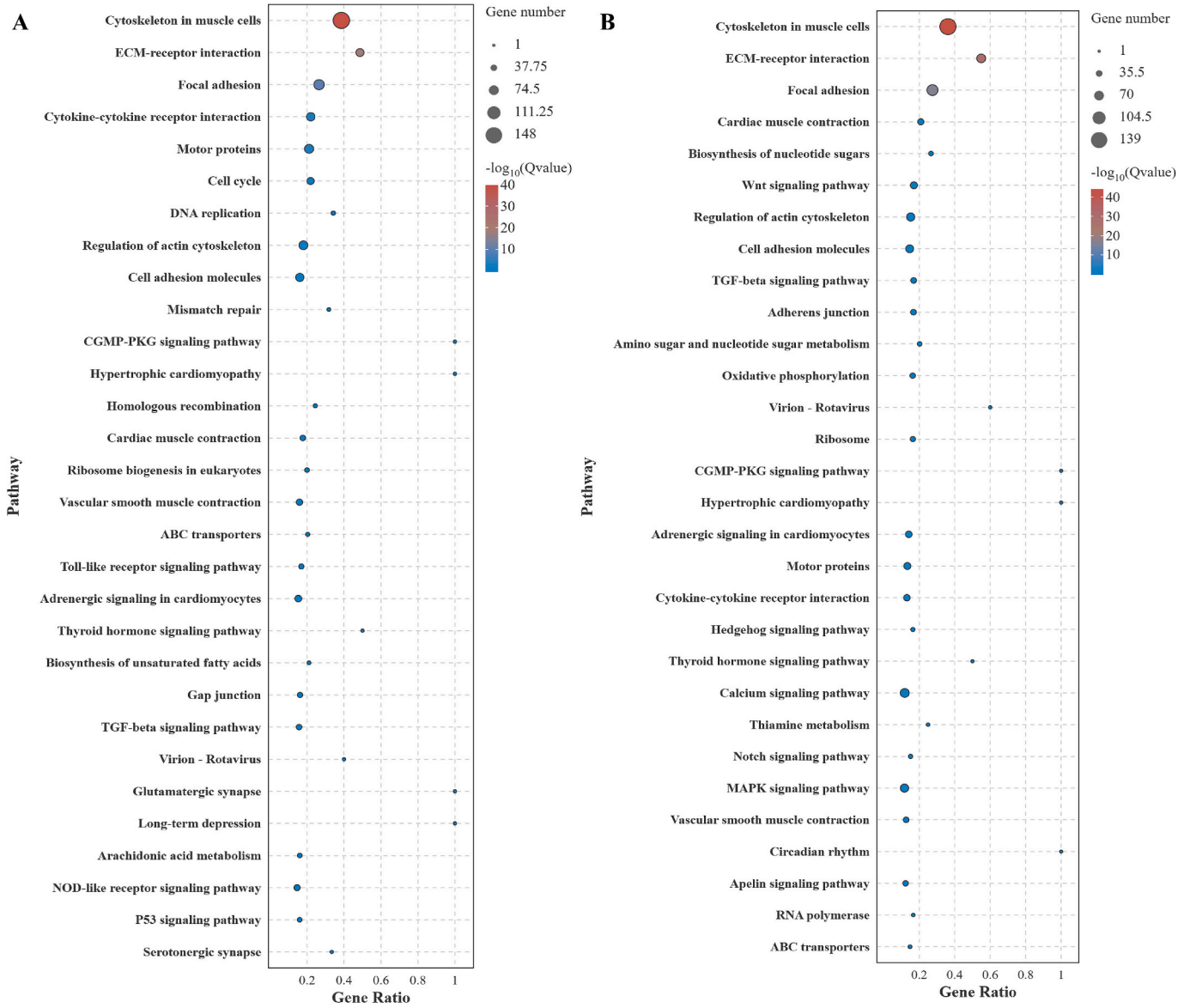


Fig. 4. GO and KEGG enrichment analyses. A: KEGG pathways enriched in DEGs for HFB-D0 vs HFB-D48. B: KEGG pathways enriched in DEGs for HFB-D48 vs HFB-R24. Transcriptomic data were analyzed using the Omicsmart online platform. Differentially expressed genes were identified according to the screening criteria described in the methods section.

min. After 3 washes with PBS, the primary antibody against BrdU (GB12051, Servicebio, China) was incubated overnight at 4 °C. After 3 washes with PBS, the slides were incubated with the secondary antibody (B100802, baipiandu, China) at room temperature in the dark for 30 min, followed by 3 washes with PBS, and air-dried. DAPI staining solution was then added and incubated in the dark for 10 min. The sections were briefly dried, mounted with anti-fluorescence quenching mounting medium (C1020, baipiandu, China), and observed under a fluorescence microscope (Nikon Eclipse C1, Nikon, Japan).

2.6. Construction and sequencing of the transcriptome library

Gill tissues collected at D0, D48 and R24 were used for RNA sequencing. RNA concentration and purity were assessed using a NanoDrop 2000 spectrophotometer (Thermo Fisher Scientific, Wilmington, DE, USA) and an Agilent 2100 Bioanalyzer (Agilent Technologies, CA, USA). RNA integrity was evaluated with the RNA Nano 6000 assay kit. mRNA was extracted and enriched using mRNA Capture Beads. After bead purification, mRNA was fragmented by high temperature. The fragmented mRNA was used as a template for first-strand cDNA synthesis in a reverse transcription reaction. During second-strand cDNA synthesis, the ends were repaired, and an A-tail was added. Next, adapters were ligated, and target fragments were selected using Hieff NGS® DNA Selection Beads. PCR amplification of the library was then performed. After quality control of the sequencing library, sequencing was conducted using the Illumina platform. Reads containing adapters were removed to obtain high-quality clean reads. The clean reads were aligned to the ribosomal database of the species using the short-read alignment tool Bowtie2. Reads mapping to the ribosomal RNA were discarded, and the remaining unmapped reads were used for subsequent transcriptome analysis. These reads were then compared to known transcripts (Genbank ID: GCF_018812025.1, *Megalobrama amblycephala*) to identify unannotated transcripts, which were functionally annotated. Gene annotation was performed using the Pfam, KEGG, eggNOG, Swiss-prot, GO, and NR databases.

Unigene expression was calculated using FPKM (fragments per kilobase of transcript per million mapped reads). Differentially expressed genes (DEGs) were identified using DESeq2. A fold change ≥2

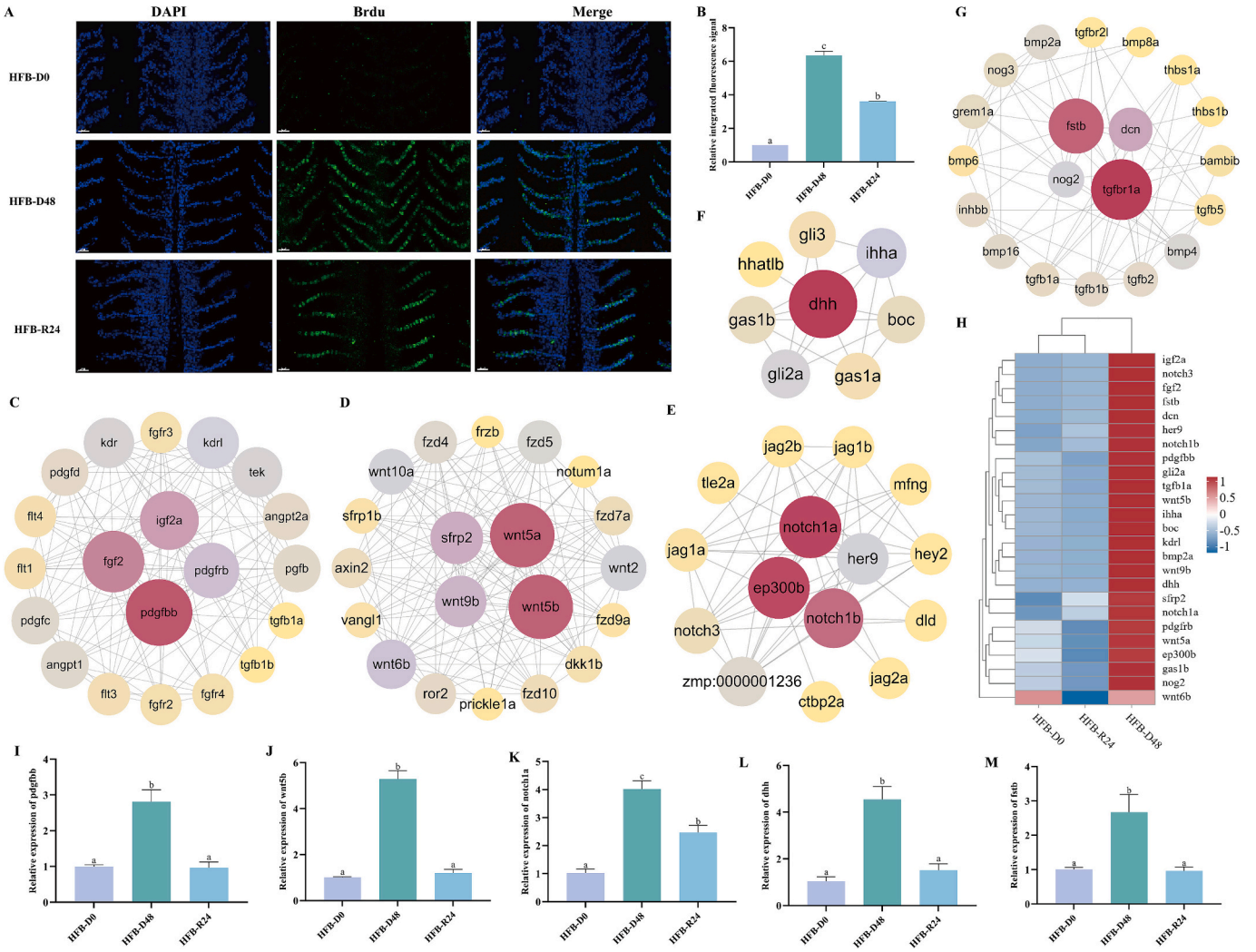


Fig. 5. Upstream pathway expression analysis regulating proliferation. A: BrdU immunofluorescence images; B: Relative integrated fluorescence signal. C: PPI of core hub genes in the MAPK signalling pathway. D: PPI of core hub genes in the Wnt signalling pathway. E: PPI of core hub genes in the Notch signalling pathway. F: PPI of core hub genes in the Hedgehog signalling pathway. G: PPI of core hub genes in the TGF-β signalling pathway. H: Heatmap analysis of genes from the five signalling pathways. I-M: Relative expression levels of genes associated with the proliferation upstream pathway; Data are presented as mean ± SEM, n = 3. Different lowercase letters indicate significant differences among groups based on one-way ANOVA followed by Duncan's multiple range test ($P < 0.05$).

and Padjust <0.05 were used as the criteria for screening DEGs. Differentially expressed genes were subjected to Gene Ontology (GO) and Kyoto Encyclopedia of Genes and Genomes (KEGG) enrichment analysis, as well as protein-protein interaction (PPI) network analysis.

2.7. PPI

Candidate proteins were first identified based on Gene Ontology (GO) and Kyoto Encyclopedia of Genes and Genomes (KEGG) enrichment analyses. Protein–protein interaction (PPI) data were then retrieved from STRING (https://cn.string-db.org/; Version:12.0) to construct the interaction network. Zebrafish (*Danio rerio*) was selected as the reference species. For the overall PPI analysis, the top 2000 DEGs (based on ascending FDR values) from the HFB-D0 vs HFB-D48 and HFB-D48 vs HFB-R24 comparison groups were used to construct two PPI networks, respectively. These networks were used to identify potential hub genes associated with hypoxia stress and reoxygenation. For the pathway-specific PPI analyses, DEGs annotated to the corresponding proliferation, structural remodelling, or immune related pathways were extracted from the relevant comparison groups and used as input genes for PPI network construction. Using the cytoHubba plugin in Cytoscape 2.8.3, genes in the PPI network were ranked, and core hub genes were subsequently screened based on betweenness centrality. In the network visualization, darker node colors indicate higher centrality, and thus greater inferred importance within the network.

2.8. Real-time quantitative PCR analysis

Total RNA was extracted from gill tissue using the TRIzol method, which was consistent with the transcriptome sequencing samples. RNA concentration was measured using a NanoDrop 2000 spectrophotometer, and RNA samples were stored at −80 °C for long-term use. Total RNA was reverse transcribed into cDNA using the PrimeScript™ RT reagent kit (TAKARA), following the instructions provided with the cDNA synthesis kit. Primers for target genes were designed using Primer-BLAST (https://www.ncbi.nlm.nih.gov/tools/primer-blast/), with 18S as the internal reference gene. The primer sequences were conserved, and primer information is provided in Table 1. According to the manufacturer's instructions, PCR was performed using the SYBR Green PCR kit (TAKARA). The PCR reactions were carried out on the CFX96 Real-Time Fluorescence Quantitative PCR System. The PCR conditions were 50 °C for 2 min, 95 °C for 10 min, followed by 40 cycles of 95 °C for 15 s and 60 °C for 1 min. The results were calculated using the $2^{-\Delta\Delta CT}$ method.

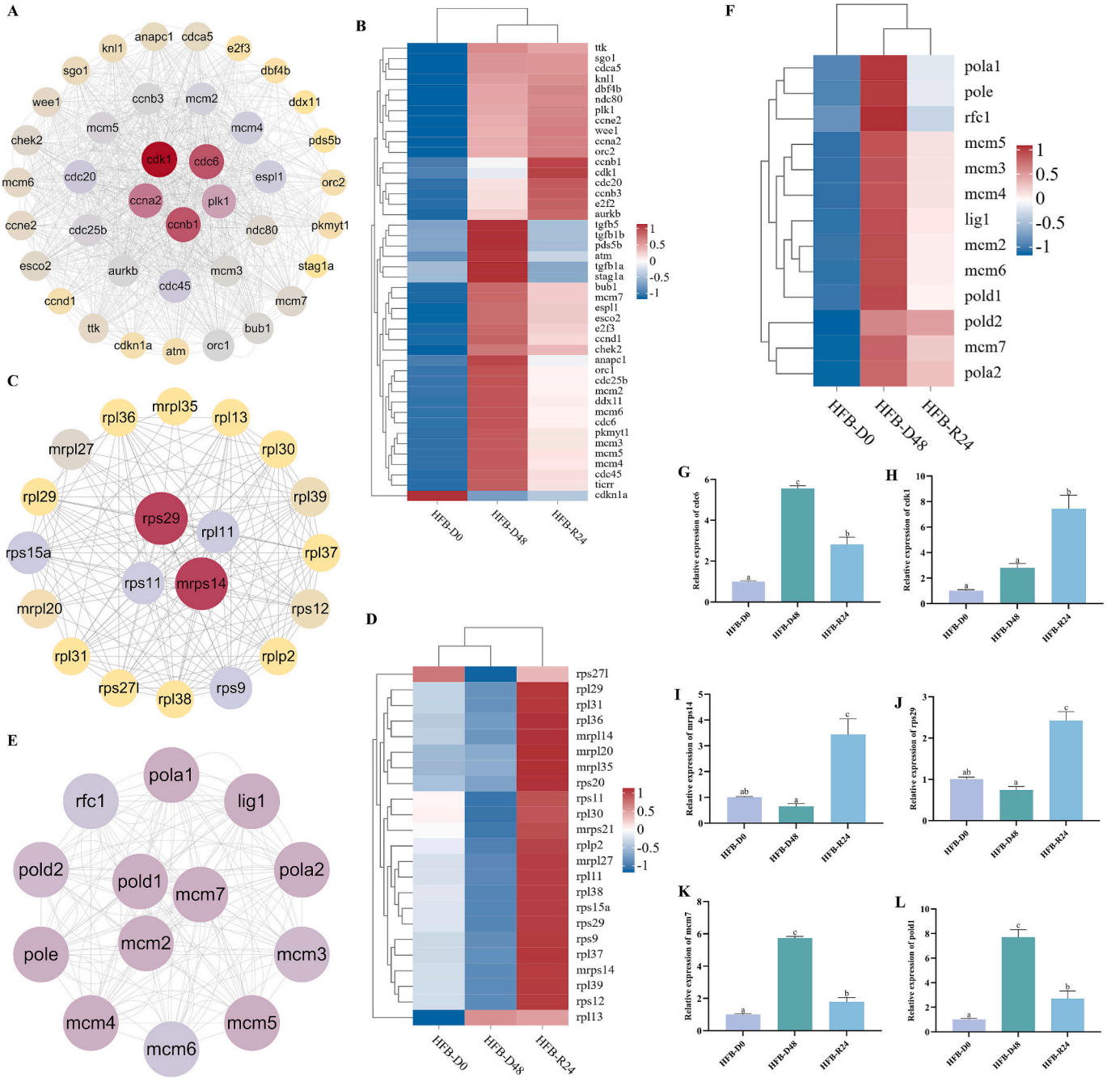


Fig. 6. Core pathway analysis related to proliferation. A–B: PPI and heatmap analysis of core hub genes in the cell cycle pathway. C–D: PPI and heatmap analysis of core hub genes in the ribosome pathway. E–F: PPI and heatmap analysis of core hub genes in the DNA replication pathway. G–L: Relative expression levels of genes associated with core proliferation pathways; Data are presented as mean ± SEM, n = 3. Different lowercase letters indicate significant differences among groups based on one-way ANOVA followed by Duncan's multiple range test ($P < 0.05$).

2.9. Data analysis

Statistical analysis of gill morphometric parameters, enzyme activity data, and qPCR-based gene expression data was performed using SPSS 26.0 software. As these datasets involved comparisons among three sampling time points, one-way analysis of variance (ANOVA) was used to test for significant differences, followed by Duncan's multiple range test for post hoc comparisons. Data are expressed as mean ± SEM, and differences were considered statistically significant at $P < 0.05$. Graphs were generated using GraphPad Prism 8. Transcriptome sequencing data were analyzed using the Omicsmart online platform (http://www.omicsmart.com), and differentially expressed genes and enrichment analyses were identified according to the criteria described in the transcriptome analysis section.

3. Results

3.1. Gill histology and enzyme activity analysis

HE staining revealed that hypoxic stress and the subsequent reoxygenation process markedly affected the gill microarchitecture (Fig. 1A). In the HFB-D0 group, the gill filaments were neatly arranged, and the secondary lamellae were intact and morphologically regular. In the HFB-D48 group, the gill tissue underwent pronounced remodelling,

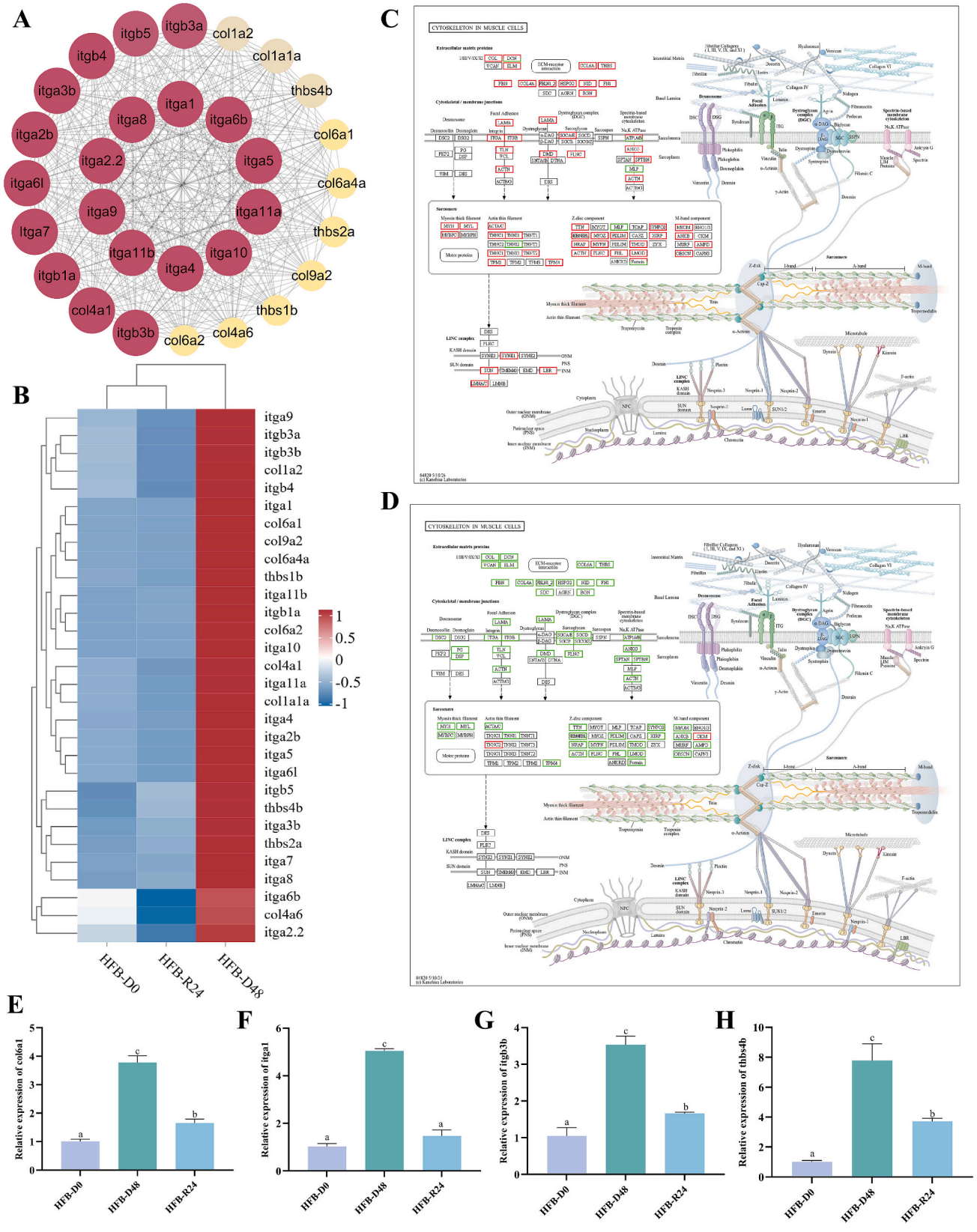


Fig. 7. Structural remodelling - Cytoskeleton in muscle cells pathway analysis. A: PPI. B: Pathway gene enrichment analysis. C–D: KEGG gene enrichment analysis of the Cytoskeleton in muscle cells signalling pathway in two comparison groups (C: HFB-D0 vs HFB-D48; D: HFB-D48 vs HFB-R24). E–H: Relative expression levels of genes associated with the cytoskeleton pathway in muscle cells; Data are presented as mean ± SEM, n = 3. Different lowercase letters indicate significant differences among groups based on one-way ANOVA followed by Duncan's multiple range test ($P < 0.05$).

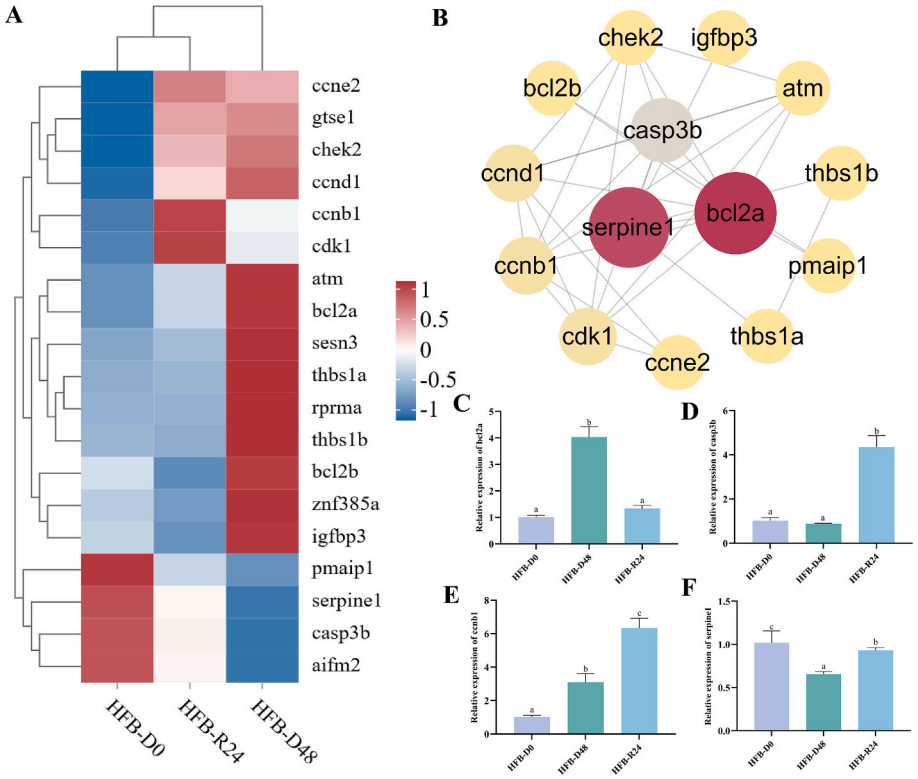


Fig. 8. P53 signalling pathway analysis. A: Gene enrichment analysis of P53 pathway-related annotated genes. B: PPI. C–F: Relative expression levels of genes associated with the P53 pathway; Data are presented as mean ± SEM, n = 3. Different lowercase letters indicate significant differences among groups based on one-way ANOVA followed by Duncan's multiple range test ($P < 0.05$).

characterized primarily by a sharp reduction in the volume of the ILCM and marked alterations in secondary lamellar morphology. After 24 h of reoxygenation, the secondary lamellae were substantially improved relative to those in the HFB-D48 group, with a more orderly cellular arrangement restored. Morphometric analyses further corroborated these observations (Table 2). Compared with the HFB-D0 group, the HFB-D48 group exhibited significant increases in PLH and PLB, whereas PLT and ILCM were significantly reduced ($P < 0.05$). The mean exposed surface area of the secondary lamellae increased significantly from (0.69×10^4) μm^2 in HFB-D0 to (3.03×10^4) μm^2 in HFB-D48 ($P < 0.05$), while ILCM volume decreased markedly from (10.39×10^4) μm^3 to (3.18×10^4) μm^3 ($P < 0.05$). By the HFB-R24 stage, these morphological parameters have shown some recovery. In addition, the activities of SOD, CAT, T-AOC, ACP and AKP were significantly elevated in the D48 group (Fig. 1 B–F; $P < 0.05$).

3.2. Basic analysis of transcriptomic differences

The PCA results showed clear separation of the three groups along the PC1 and PC2 axes, with no overlap and good dispersion, indicating that the three treatments represented independent and markedly distinct physiological states (Fig. 2A). In the HFB-D0 vs HFB-D48 comparison, a total of 3160 significantly differentially expressed genes (DEGs) were identified, of which 2292 were upregulated and 868 were downregulated (Fig. 2B). In the HFB-D48 vs HFB-R24 comparison, 2399 DEGs were detected, including 532 upregulated and 1867 downregulated genes (Fig. 2C). The sample-to-sample correlation heatmap revealed consistently high correlations among all pairs of samples, demonstrating strong internal consistency within the dataset (Fig. 2D). Venn analysis further showed that 1829 DEGs were unique to the HFB-D0 vs HFB-D48 comparison, whereas 1068 DEGs were unique to the HFB-D48 vs HFB-R24 comparison (Fig. 2E).

3.3. GO and KEGG enrichment analyses

GO enrichment analysis indicated that, in the HFB-D0 vs HFB-D48 comparison, DEGs were significantly enriched in terms related to cellular structure and angiogenesis (Fig. 3A), including cell adhesion, Extracellular matrix organization, blood vessel development, and angiogenesis. In the HFB-D48 vs HFB-R24 comparison (Fig. 3B), DEGs were likewise significantly enriched in terms associated with ECM remodelling (such as extracellular matrix organization and cell adhesion) and vascular system repair. In addition, development-related terms, including anatomical structure morphogenesis and tissue development, were also significantly enriched. KEGG pathway enrichment analysis further revealed the potential molecular process (Fig. 4). During both hypoxia and reoxygenation stages, the pathways related to cytoskeleton in muscle cells, ECM-receptor interaction, focal adhesion, and cytokine-cytokine receptor interaction were all significantly activated. Specifically, hypoxic stress triggered core proliferation pathways, including the cell cycle and DNA replication, and activated Toll-like receptor and NOD-like receptor-mediated innate immune responses. Additionally, the P53 signalling pathway, which is associated with apoptosis, was significantly enriched (Fig. 4A). During reoxygenation, pathways such as Wnt, TGF-β, MAPK, and Notch were significantly activated. Notably, the ribosome pathway was significantly enriched during the reoxygenation phase (Fig. 4B).

3.4. Analysis of proliferation-related pathways

Immunofluorescence (IF) results visually demonstrated changes in cell proliferation activity (Fig. 5A). The HFB-D48 group exhibited dense proliferating cell signals, with a relative integrated fluorescence signal approximately 6.4 times that of the HFB-D0 group ($P < 0.05$) (Fig. 5B). Following reoxygenation, fluorescence intensity significantly decreased but remained at 3.6 times the level of the HFB-D0 group ($P < 0.05$).

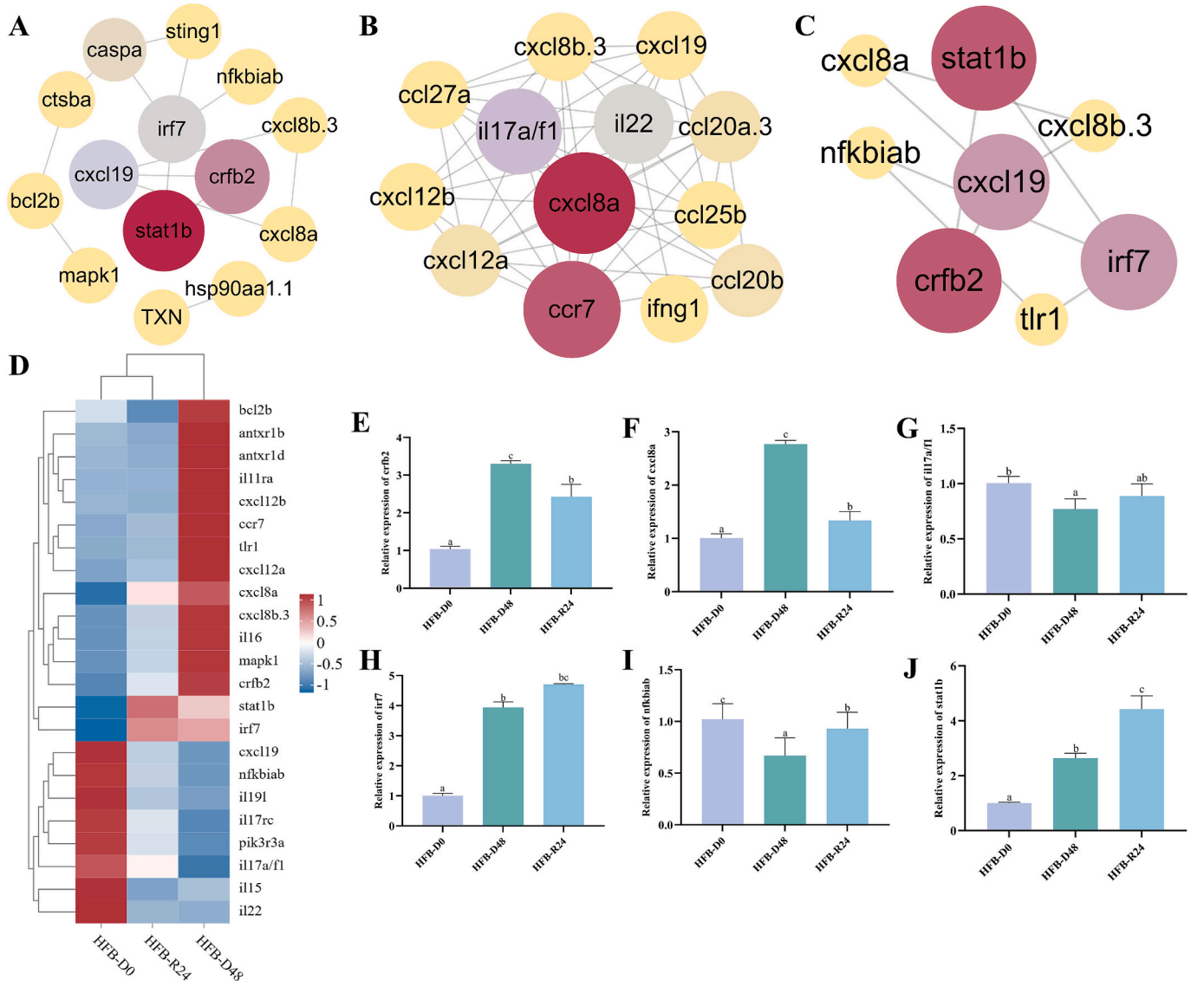


Fig. 9. Immune inflammation-related pathway analysis. A: PPI of core hub genes in the NOD-like receptor pathway. B: PPI of core hub genes in the Cytokine-cytokine receptor interaction pathway. C: PPI of core hub genes in the Toll-like receptor signalling pathway. D: Gene enrichment analysis of immune inflammation-related pathways. E-J: Relative expression levels of genes in immune-related pathways; Data are presented as mean ± SEM, n = 3. Different lowercase letters indicate significant differences among groups based on one-way ANOVA followed by Duncan's multiple range test ($P < 0.05$).

KEGG enrichment analysis of upstream signalling pathways regulating proliferation (MAPK/Wnt/Notch/TGF-β/Hedgehog) revealed that the expression of core genes in these pathways was upregulated in the HFB-D48 group (Fig. 5C–H). Core genes related to downstream pathways driving proliferation, such as the cell cycle (Fig. 6A, D) and DNA replication (Fig. 6C, F), were activated during hypoxia, further triggering compensatory proliferation in gill tissue. In contrast, ribosome pathway genes were upregulated in the HFB-R24 group during reoxygenation.

3.5. Analysis of pathways related to structural remodelling and apoptosis

The pathways related to structural remodelling, represented by the cytoskeleton in muscle cells, are shown in Fig. 7. All genes annotated in this pathway were upregulated in the HFB-D48 group, and PPI analysis revealed that the *Itga* family genes served as key hub genes in this pathway (Fig. 7A, B). The specific distribution of differentially expressed genes in the Cytoskeleton in muscle cells pathway between the two comparison groups is shown in Fig. 7C, D. In the P53 signalling pathway analysis, the genes *bcl2a*, *bcl2b*, and *sesn3* were highly expressed in the HFB-D48 group, while *pmaip1*, *casp3b*, and *aifm2* were downregulated in the HFB-D48 group. The genes *bcl2a*, *serpine1*, and *casp3b* were identified as key hub genes in this pathway (Fig. 8).

3.6. Analysis of immune and inflammatory-related pathways

In this study, three immune and inflammation-related pathways were selected (Fig. 9). As shown in the figure, chemokines (*cxcl8a*, *cxcl8b.3*, *cxcl12a/b*) and their receptors (*ccr7*), along with damage-sensing receptors (*tlr1*), were significantly enriched in the D48 group. The NF-κB inhibitor (*nfkbiab*) was highly expressed in the D0 group but downregulated in the D48 group. Meanwhile, cytokines responsible for maintaining mucosal barrier homeostasis (*il17a/f1*, *il22*, *il15*) were significantly suppressed under hypoxic conditions. During reoxygenation, although most pro-inflammatory factors decreased, interferon regulatory factors (*irf7*, *stat1b*) continued to maintain relatively high expression levels.

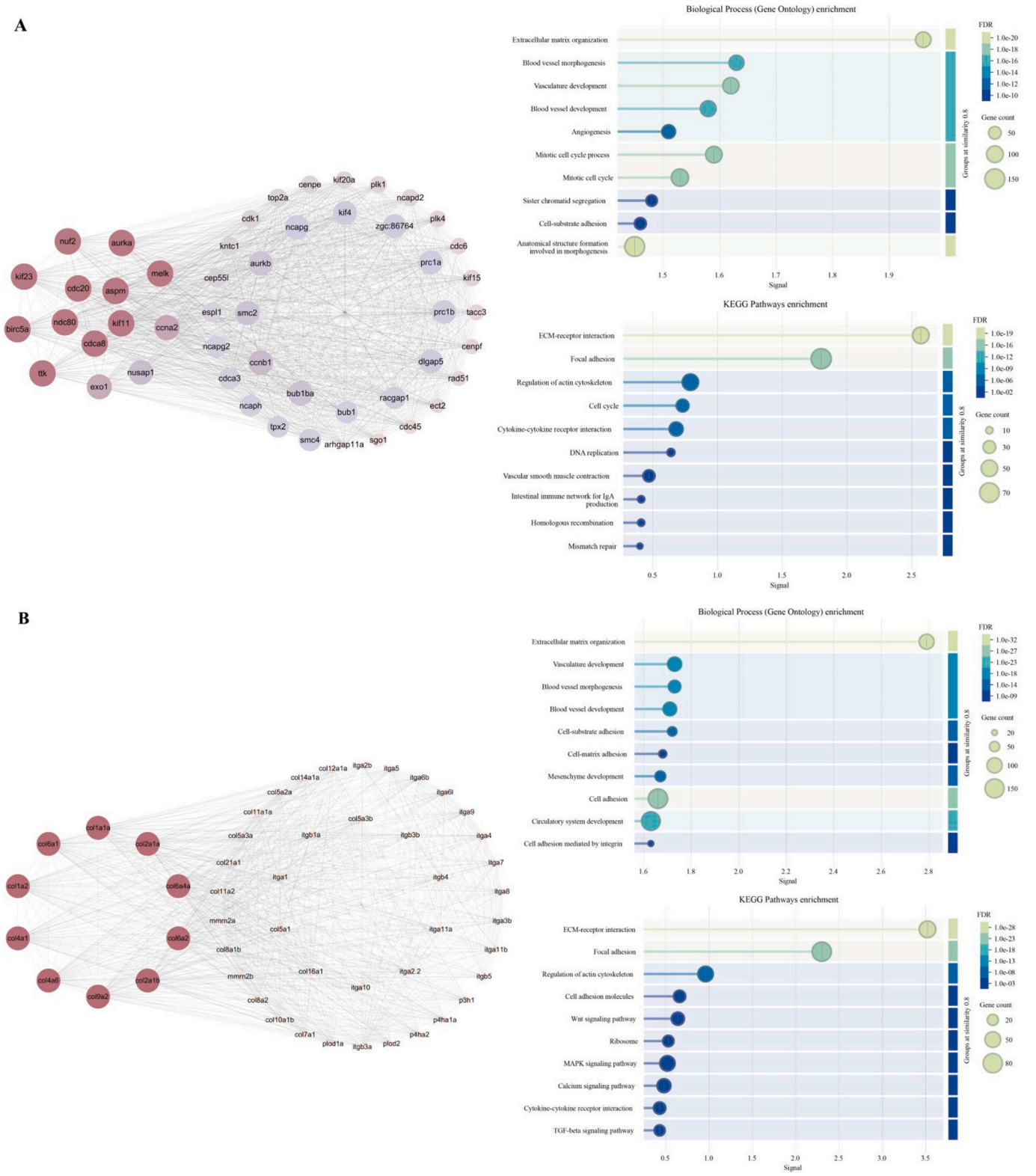


Fig. 10. PPI network and functional annotation analysis of DEGs in the transcriptome during hypoxia and reoxygenation phases (Top 50). A: HFB-D0 vs HFB-D48. B: HFB-D48 vs HFB-R24.

3.7. PPI analysis of transcriptomic DEGs

To identify key regulatory factors, a PPI analysis and annotation were performed on the top 2000 DEGs (based on ascending FDR values) from the two comparison groups. The top 50 core genes were selected to construct the PPI network, followed by temporal expression clustering analysis. During the hypoxic response phase, the core hub genes in the network were primarily involved in cell cycle regulation, including *cdk1*, *aurka*, *plk1*, and *birc5a* (Fig. 10A). In contrast, the core hub genes during the reoxygenation phase were mainly focused on ECM components, such as *col1a1a*, *col4a1*, *col1a2*, and *col6a1* (Fig. 10B). Functional annotation of the PPI network further revealed that GO annotation

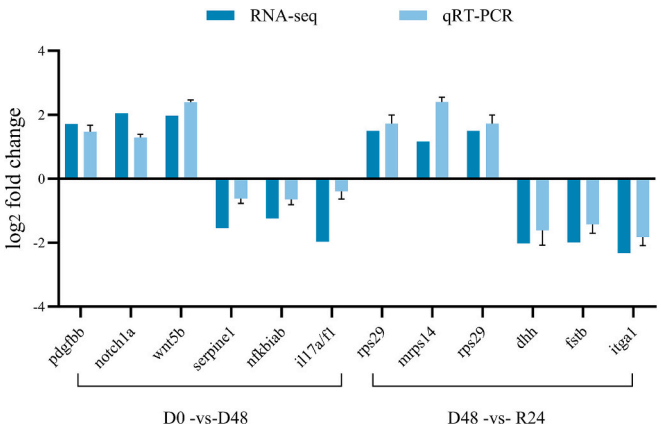


Fig. 11. PPI network and functional annotation analysis of DEGs in the transcriptome during hypoxia and reoxygenation phases (Top 50). A: HFB-D0 vs HFB-D48. B: HFB-D48 vs HFB-R24.

identified extracellular matrix organization and blood vessel development as dominant terms during both hypoxic stress and reoxygenation. KEGG annotation results indicated that the ECM-receptor interaction and focal adhesion pathways were predominant during both hypoxia and reoxygenation. All of these pathways are associated with proliferation. To verify the reliability of the RNA-seq data, several DEGs from the two comparison groups were selected for qRT-PCR analysis. The expression change trends of these genes were largely consistent between the RNA-seq and qRT-PCR results (Fig. 11).

4. Discussion

The gills are the primary organs for gas exchange in fish, capable of adaptive regulation in response to fluctuations in dissolved oxygen levels (Evans et al., 2005). Previous studies have reported that blunt snout bream is relatively sensitive to hypoxia. Hypoxic stress can induce gill structural injury, apoptosis-related responses, and changes in the expression of hypoxia-related genes (Yu et al., 2023). In another study, the F3 hybrid progeny derived from *Megalobrama terminalis* (♂) and *Culter alburnus* (♀) exhibited greater hypoxia tolerance than *Megalobrama terminalis*. Moreover, the F3 population showed a stronger capacity for gill remodelling than *Megalobrama terminalis* (Chen et al., 2023). Cheng et al. (2025) found that the hybrid CM, derived from *Culter alburnus* (♀) and *Megalobrama terminalis* (♂), may exhibit greater hypoxia tolerance than *Culter alburnus*. Compared with *Culter alburnus*, CM showed a lower oxygen demand at 25 °C, accompanied by increased activities of SOD and GSH enzymes (Cheng et al., 2025). A recent study showed that the hypoxia tolerance of HFB was 33.3% higher than that of *Megalobrama terminalis* (Wen et al., 2025). Similarly, a study on cyprinid fish showed that the F1 hybrid population exhibited intermediate hypoxia tolerance between the two parental strains, with higher tolerance than the hypoxia-sensitive parent, suggesting a potential hybrid advantage in hypoxia adaptation (Suo et al., 2022). Chen et al. (2022) reported in *Gymnocypris przewalskii* that hypoxic stress disrupts gill tissue morphology, accompanied by marked elevations in total antioxidant capacity and glutathione peroxidase activity (Chen et al., 2022). In another study, hypoxic stress induced pronounced morphological remodelling in the gills of *Sebastes schlegelii* (Jia et al., 2021). This study first focused on the gill tissue response of HFB under hypoxic stress. Morphological analysis indicates that the gill tissue of HFB exhibits significant reversibility under hypoxic stress conditions. Hypoxia led to an increase in gill lamellae surface area, a decrease in lamellae thickness, and a reduction in interlamellar cell mass. These parameters largely recovered 24 h after reoxygenation, indicating significant reversibility in gill structure. Additionally, we further observed a significant increase in antioxidant enzyme activity in the HFB-D48 group.

Fish gills are highly plastic organs that can rapidly remodel to expand the respiratory surface area in response to environmental hypoxia (Gilmour and Turko, 2024). In the present study, immunofluorescence (IF) provided direct visual evidence for this plasticity. Relative to the HFB-D0 group, the HFB-D48 group exhibited a 6.4-fold surge in

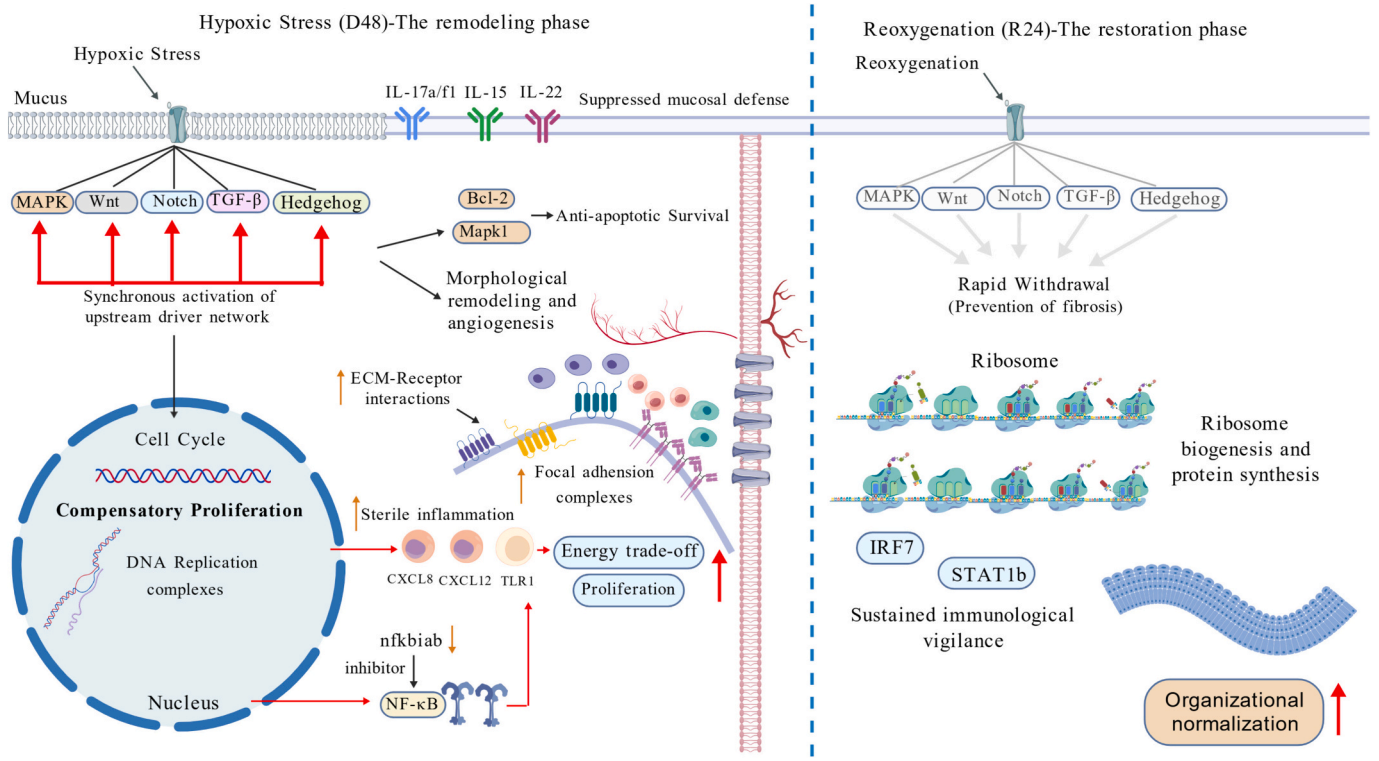


Fig. 12. Key signalling pathway network involved in Hefang bream's response to hypoxia-induced structural remodelling and reoxygenation recovery.

proliferating-cell signal. This robust proliferative response indicates that HFB enhances oxygen uptake during acute hypoxic stress by inducing compensatory gill remodelling, a critical factor contributing to its superior hypoxia tolerance. Therefore, by integrating transcriptomics, protein-protein interaction network analysis, and functional enrichment analysis, we aim to identify key molecular networks involved in hypoxic stress and reoxygenation. The Wnt signalling pathway promotes the accumulation of β-catenin in the cytoplasm and nucleus, thereby activating the transcription of key targets such as Cyclin D1 and C-myc. In addition to regulating the cell cycle, this pathway promotes tissue growth during embryonic development and maintains the equilibrium of haematopoietic stem cells (Hayat et al., 2022). The MAPK signalling pathway is an indispensable regulatory hub in organ regeneration. It rapidly activates after injury, regulating cell survival, migration, proliferation, and growth (Wen et al., 2022). The TGF-β signalling pathway is activated primarily through SMAD-dependent mechanisms and, following injury, promotes cell proliferation, migration and extracellular matrix remodelling (Gumede et al., 2024). During tissue repair, Notch signalling promotes angiogenesis by recruiting M1 macrophages and inducing the expression of IL-6 and VEGFR (Zhou et al., 2022). The Hedgehog signalling pathway is a core regulator of embryonic tissue patterning, postnatal tissue regeneration and stem-cell function, and it plays a pivotal role in controlling cell proliferation and development (Zhang and Beachy, 2023). Our study found that multiple upstream proliferative signalling pathways-MAPK, Wnt, Notch, TGF-β, and Hedgehog-were coordinately upregulated in the HFB-D48 group. Transcriptome analysis further corroborated this phenotype, revealing that core pathways driving cell division (cell cycle and DNA replication) were significantly activated at the D48 stage. This provides a cellular source for the morphological changes in gill lamellae at the molecular level. This indicates that the HFB regulates gill remodelling through a complex process, thereby ensuring survival during hypoxic stress.

The change of gill morphology is manifested by the activation of Cytoskeleton pathways in muscle cells at the KEGG level. ITGA proteins serve as key bridges linking the extracellular matrix (ECM) to the intracellular actin cytoskeleton (Coelho et al., 2006). Proteins encoded by the integrin (ITGA) family are heterodimeric receptors on the cell surface that play central roles in cell adhesion, signal transduction and cell-microenvironment interactions (Zhu et al., 2020). PPI network analysis identified ITGA family proteins as the hub proteins within this signalling pathway. Given the widespread activation of ITGA family genes, we hypothesize that hypoxic signalling may be transduced via integrin-mediated transmembrane signalling to activate focal adhesion kinase (FAK), subsequently triggering actin cytoskeleton rearrangement within pillar cells. Pillar cells, as the key cells supporting the structure of gill lamellae, directly shorten the distance for gas diffusion through their contraction or morphological changes. This reduces the diffusion distance for oxygen and increases the effective respiratory surface area (Jonz, 2024). The activation of cell adhesion pathways may be essential for maintaining the integrity of the epithelial barrier during the remodelling process, preventing the loss of tissue integrity caused by drastic morphological changes (Abedin and King, 2010).

In classical biological logic, the P53 pathway is typically associated with cell cycle arrest or apoptosis (Wang et al., 2023). In numerous fish studies, prolonged hypoxia typically activates the P53 pathway, leading to severe cell cycle arrest or even apoptosis (Mai et al., 2010; Qiang et al., 2020; Wang et al., 2022; Xiao, 2015). In this study, HFB similarly activated the P53 pathway following hypoxic stress. However, the downstream classical apoptosis pathway did not show significant upregulation. This indicates that the activation of P53 is primarily utilized to induce temporary cell cycle checkpoint arrest for DNA repair. Similarly, in studies on *Carassius auratus*, activation of the P53 signalling pathway under hypoxic stress has also been observed (Xing et al., 2025). The upregulation of Bcl-2 family proteins effectively counteracts cell death induced by the mitochondrial pathway (Saddam et al., 2024), while Sesn3 is responsible for clearing the accumulation of reactive oxygen species (ROS) generated under hypoxia (Chen et al., 2025). The hub genes *bcl2a* and *casp3b* identified through PPI analysis further confirm the core function of the P53 pathway under hypoxia. These findings suggest that the pathway does not eliminate damaged cells, but rather safeguards the survival of the remodelling gill tissue by lowering the apoptotic threshold. This strategy enables HFB to maximize structural remodelling while circumventing the induction of widespread apoptosis. Beyond the remodelling of physical barriers, adaptive regulation of the vasculature constitutes another key mechanism for ensuring oxygen delivery under hypoxic conditions. GO and KEGG enrichment analyses identified multiple pathways associated with angiogenesis. Under hypoxic conditions, in addition to the formation of new blood vessels, rapid adjustment of the diameter of existing vessels serves as a more immediate compensatory mechanism. The CGMP-PKG pathway is a classic nitric oxide (NO)-dependent vasodilation pathway (Gambaryan, 2022). Enrichment of this pathway suggests that HFB gill tissue may upregulate NO synthesis, activate the cGMP-PKG signalling, and induce vasodilation of gill vascular smooth muscle. This would reduce vascular resistance and increase blood flow across the respiratory surface. This rapid vasodilation, combined with newly formed vessels, ensures adequate blood perfusion and oxygen uptake in hypoxic environments. A similar phenomenon was observed in the study on *Seriola dumerili* (Li et al., 2024).

However, although the changes of gill morphology under hypoxia stress enhance the oxygen uptake capacity, it may also increase the risk of pathogen invasion (Nilsson, 2007). Our study found that *nfkbiab*, the endogenous inhibitor of the NF-κB signalling pathway, is highly expressed under normoxic conditions. However, this expression is significantly downregulated under hypoxic stress. Under hypoxic stress, the down-regulation of *nfkbiab* directly drives the transcriptional activation of downstream pro-inflammatory cytokines and chemokines. Notably, the significant enrichment of *cxcl8* and *cxcl12* indicates the initiation of a robust sterile inflammatory response. Via CCR7- and TLR1-mediated signalling pathways, immune cells are driven to migrate to damaged tissues. This provides the necessary microenvironment for subsequent structural remodelling and tissue repair. This substantiates that HFB employs an active defense strategy under hypoxic stress, rather than undergoing passive damage. In the study on hybrid yellow catfish, it was found that genes related to the NOD-like receptor signalling pathway were rapidly upregulated at the early stages of hypoxic stress, followed by a decline over time (Tao et al., 2021). This is consistent with the findings of the present study.

To further identify key regulatory factors driving hypoxia- and reoxygenation-induced gill remodelling, we constructed a PPI network of differentially expressed genes. During the hypoxic response phase, the core of the network was dominated by genes such as *cdk1*, *aurka*, *plk1* and *birc5a*. Among these, *cdk1* encodes the central kinase that drives entry into mitosis (Enserink and Kolodner, 2010; Gavet and Pines, 2010). In contrast, *aurka* and *plk1* play pivotal roles in spindle assembly and chromosome segregation (Asteriti et al., 2015). This finding further corroborates, at the level of protein-protein interactions, the compensatory proliferation observed at the HFB-D48 stage. This cell cycle-centered response ensures the rapid generation of new gill cells during the early stages of hypoxia. This provides the necessary cellular reservoir for the expansion of the gill lamellar surface area. Collagens are major constituents of the extracellular matrix (ECM), providing tissues with mechanical strength and structural support (Karamanos et al., 2021). Following reoxygenation, the core hubs of the PPI network rapidly shifted to collagen-family genes, including *col1a1a*, *col4a1*, *col1a2* and *col6a1*. This suggests that the organism is prioritizing the repair of capillaries and the basement membrane beneath the epithelial cells. Integrins serve as the primary cell-surface receptors for the ECM. In the PPI network, they form dense connections with collagens, indicating that newly synthesized collagens are being recognized and bound by integrins on the cell membrane.

Through histological and transcriptomic analyses, this study

revealed the adaptive process of HFB gill tissue during hypoxic stress and reoxygenation, as illustrated in Fig. 12. Hypoxic stress altered gill morphology and structure, while enhancing antioxidant and immune enzyme activities. In response to hypoxic stress, the organism first activated upstream proliferation and morphogenesis signalling networks. These networks then drove downstream cell cycle and DNA replication processes, ultimately resulting in compensatory cell proliferation. Subsequently, pathways related to structural remodelling and angiogenesis were activated. This confirms that the organism maximizes its oxygen uptake capacity through active morphological remodelling and the construction of a vascular network. Immune responses were characterized by the downregulation of the NF-κB inhibitor. This downregulation induced a sterile inflammation driven by the TLR pathway and chemokines to facilitate tissue repair. During reoxygenation, the focus turns to structural remodelling and immune regulation to restore body balance. This study reveals the regulatory mechanism of gill tissue in HFB during hypoxia stress and reoxygenation, providing new insights into the adaptive basis of HFB hypoxia tolerance.

CRediT authorship contribution statement

Xinxin Yu: Writing – original draft, Methodology, Data curation. **Minghui Xiao:** Formal analysis, Conceptualization. **Siyu Fan:** Visualization. **Zhifeng Zhou:** Visualization. **Zhong Tang:** Software. **Ming Wen:** Validation. **Shengnan Li:** Software. **Yuequn Wang:** Validation. **Min Tao:** Writing – review & editing, Resources, Project administration, Funding acquisition. **Shaojun Liu:** Writing – review & editing, Resources, Project administration, Funding acquisition.

Funding

This work was financially supported by the National Key Research and Development Program of China (2022YFD2400600/2022YFD2400601), the Science and Technology Innovation Program of Hunan Province (Grant No. 2023RC1053), the National Natural Science Foundation of China (Grant No. 32293253), the Yuelushan Laboratory Breeding Program (Grant No. YLS-2025-ZY01011), and the Earmarked Fund for Agriculture Research System of China (CARS-45).

Declaration of competing interest

All authors declare that they have no conflict of interest.

Data availability

Data will be made available on request. All raw transcriptomic sequencing data have been deposited in the NCBI database under accession number PRJNA1464224.

References

Abedin, M., King, N., 2010. Diverse evolutionary paths to cell adhesion. Trends Cell Biol. 20 (12), 734–742. https://doi.org/10.1016/j.tcb.2010.08.002.

Asteriti, I.A., De Mattia, F., Guarguaglini, G., 2015. Cross-talk between aurka and plk1 in mitotic entry and spindle assembly. Front. Oncol. 5. https://doi.org/10.3389/fonc.2015.00283.

Bickler, P.E., Buck, L.T., 2007. Hypoxia tolerance in reptiles, amphibians, and fishes: life with variable oxygen availability. Annu. Rev. Physiol. 69, 145–170. https://doi.org/10.1146/annurev.physiol.69.031905.162529.

Bundgaard, A., Ruhr, I.M., Fago, A., Galli, G.L.J., 2020. Metabolic adaptations to anoxia and reoxygenation: new lessons from freshwater turtles and *Crucian carp*. Curr. Opin. Endocr. Metab. Res. 11, 55–64. https://doi.org/10.1016/j.coemr.2020.01.002.

Chen, F.J., Ling, X.D., Zhao, Y.T., Fu, S.Y., 2022. Hypoxia-induced oxidative stress and apoptosis in gills of scaleless carp (*Gymnocypris przewalskii*). Fish Physiol. Biochem. 48 (4), 911–924. https://doi.org/10.1007/s10695-022-01091-3.

Chen, S.L., Xu, W.Y., Shuang, L., Wen, J., Zheng, G.D., Zou, S.M., 2023. Evaluation of hypoxia tolerance in F3 hybrids of blunt snout bream (*Megalobrama amblycephala* ♀) × topmouth culter (*Culter alburnus* ♂). Aquaculture 573. https://doi.org/10.1016/j.aquaculture.2023.739589.

Chen, Q.S., Zhong, G.Q., Fang, X.M., Lin, C.Z., Wang, S.P., Li, M.S., 2025. The multifaceted role of sestrin 3 (sesn3) in oxidative stress, inflammation and tumorigenesis. Biochim. Biophys. Acta 1872 (5). https://doi.org/10.1016/j.bbamcr.2025.119938.

Cheng, S., Zhang, M.F., Jiang, W.P., Chi, M.L., Zheng, J.B., Liu, S.L., Hang, X.Y., Peng, M., Li, F., 2025. Study on morphological characteristics and hypoxia tolerance of *Culter alburnus* (♀) × *Magalobrama terminalis* (♂) and *Culter alburnus*. Isr. J. Aquacult. Bamid 77 (3), 124–133. https://doi.org/10.46989/001c.138331.

Coelho, L.F.L., Mota, B.E.F., Sales, P.C.M., Marques, J.T., de Oliveira, J.G., Bonjardim, C. A., Ferreira, P.C.P., Kroon, E.G., 2006. Integrin alpha 11 is a novel type i interferon stimulated gene. Cytokine 33 (6), 352–361. https://doi.org/10.1016/j.cyto.2006.03.007.

Dagoudo, M., Qiang, J., Bao, J.W., Tao, Y.F., Zhu, T.H.J., Tumukunde, E.M., Ngoepe, T. K., Xu, P., 2021. Effects of acute hypoxia stress on hemato-biochemical parameters, oxidative resistance ability, and immune responses of hybrid yellow catfish (*Pelteobagrus fulvidraco* × *P. vachelli*) juveniles. Aquac. Int. 29 (5), 2181–2196. https://doi.org/10.1007/s10499-021-00742-1.

Dhillon, R.S., Yao, L., Matey, V., Chen, B.J., Zhang, A.J., Cao, Z.D., Fu, S.J., Brauner, C.J., Wang, Y.S., Richards, J.G., 2013. Interspecific differences in hypoxia-induced gill remodelling in carp. Physiol. Biochem. Zool. 86 (6), 727–739. https://doi.org/10.1086/673180.

Enserink, J.M., Kolodner, R.D., 2010. An overview of cdk1-controlled targets and processes. Cell Div. 5. https://doi.org/10.1186/1747-1028-5-11.

Evans, D.H., Piermarini, P.M., Choe, K.P., 2005. The multifunctional fish gill: dominant site of gas exchange, osmoregulation, acid-base regulation, and excretion of nitrogenous waste. Physiol. Rev. 85 (1), 97–177. https://doi.org/10.1152/physrev.00050.2003.

Gambaryan, S., 2022. The role of no/sgc/cgmp/pkg signalling pathway in regulation of platelet function. Cells 11 (22). https://doi.org/10.3390/cells11223704.

Gavet, O., Pines, J., 2010. Activation of cyclin b1-cdk1 synchronizes events in the nucleus and the cytoplasm at mitosis. J. Cell Biol. 189 (2), 247–259. https://doi.org/10.1083/jcb.200909144.

Gilmour, K.M., Turko, A.J., 2024. Effects of structural remodelling on gill physiology. J. Comp. Physiol. B. 194 (5), 595–609. https://doi.org/10.1007/s00360-024-01558-0.

Gong, D., Xu, L., Liu, Q., Wang, S., Wang, Y., Hu, F., Wu, C., Luo, K., Tang, C., Zhou, R., Zhang, C., Tao, M., Wang, Y., Liu, S., 2021. A new type of hybrid bream derived from a hybrid lineage of *Megalobrama amblycephala* (♀) × *Culter alburnus* (♂). Aquaculture 534. https://doi.org/10.1016/j.aquaculture.2020.736194.

Gumede, D.B., Abrahamse, H., Houreld, N.N., 2024. Targeting wnt/β-catenin signalling and its interplay with tgf-β and notch signalling pathways for the treatment of chronic wounds. Cell Commun. Signal 22 (1). https://doi.org/10.1186/s12964-024-01623-9.

Halina, F., Sokolova, Inna M., 2023. Intermittent hypoxia differentially affects metabolic and oxidative stress responses in two species of cyprinid fish. Biol. Open 12 (9). https://doi.org/10.1242/bio.060069.

Hayat, R., Manzoor, M., Hussain, A., 2022. Wnt signalling pathway: a comprehensive review. Cell Biol. Int. 46 (6), 863–877. https://doi.org/10.1002/cbin.11797.

Jia, Y.D., Gao, Y.T., Wan, J.M., Gao, Y.H., Li, J., Guan, C.T., 2021. Altered physiological response and gill histology in black rockfish, *Sebastes schlegelii*, during progressive hypoxia and reoxygenation. Fish Physiol. Biochem. 47 (4), 1133–1147. https://doi.org/10.1007/s10695-021-00970-5.

Jonz, M.G., 2024. Cell proliferation and regeneration in the gill. J. Comp. Physiol. B. 194 (5), 583–593. https://doi.org/10.1007/s00360-024-01548-2.

Karamanos, N.K., Theocharis, A.D., Piperigkou, Z., Manou, D., Passi, A., Skandalis, S.S., Vynios, D.H., Orian-Rousseau, V., Ricard-Blum, S., Schmelzer, C.E.H., Duca, L., Durbee, M., Afratis, N.A., Troeberg, L., Franchi, M., Masola, V., Onisto, M., 2021. A guide to the composition and functions of the extracellular matrix. FEBS J. 288 (24), 6850–6912. https://doi.org/10.1111/febs.15776.

Li, X.H., Ling, C., Wang, Q.X., Feng, C., Luo, X.Z., Sha, H., He, G.Y., Zou, G.W., Liang, H. W., 2022. Hypoxia stress induces tissue damage, immune defense, and oxygen transport change in gill of silver carp (*Hypophthalmichthys molitrix*): evaluation on hypoxia by using transcriptomics. Front. Mar. Sci. 9. https://doi.org/10.3389/fmars.2022.900200.

Li, D., Zhang, W.W., Wang, T., Yang, Y., Hua, S.J., Ruan, Q.X., Wang, X., Zhu, C.H., Meng, Z.N., 2024. Hypoxia stress alters gene expression in the gills and spleen of greater amberjack (*Seriola dumerili*). Fish Shellfish Immunol. 150. https://doi.org/10.1016/j.fsi.2024.109602.

Liu, Q., Guo, L.P., Zhang, H.W., Ge, J.Y., Luo, J., Song, K.G., Zhao, L.L., Yang, S., 2024. Hypoxia induces reversible gill remodeling in largemouth bass (*Micropterus salmoides*) through integrins-mediated cell adhesion. Fish Shellfish Immunol. 154. https://doi.org/10.1016/j.fsi.2024.109918.

Ma, J.L., Xu, D.P., Tao, Y.F., Zheng, T., Xu, P., Qiang, J., 2023. Integrated transcriptome and miRNA sequencing analyses reveal that hypoxia stress induces immune and metabolic disorders in gill of genetically improved farmed tilapia (GIFT, *Oreochromis niloticus*). Fish Shellfish Immunol. 139. https://doi.org/10.1016/j.fsi.2023.108909.

Mai, W.J., Yan, J.L., Wang, L., Zheng, Y., Xin, Y., Wang, W.N., 2010. Acute acidic exposure induces p53-mediated oxidative stress and DNA damage in tilapia (*Oreochromis niloticus*) blood cells. Aquat. Toxicol. 100 (3), 271–281. https://doi.org/10.1016/j.aquatox.2010.07.025.

Matey, V., Richards, J.G., Wang, Y.X., Wood, C.M., Rogers, J., Davies, R., Murray, B.W., Chen, X.Q., Du, J.Z., Brauner, C.J., 2008. The effect of hypoxia on gill morphology and ionoregulatory status in the Lake Qinghai scaleless carp, *Gymnocypris przewalskii*. J. Exp. Biol. 211 (7), 1063–1074. https://doi.org/10.1242/jeb.010181.

Nilsson, G.E., 2007. Gill remodelling in fish-a new fashion or an ancient secret? J. Exp. Biol. 210 (Pt 14), 2403–2409. https://doi.org/10.1242/jeb.000281.

Nilsson, G.E., Renshaw, G.M., 2004. Hypoxic survival strategies in two fishes: extreme anoxia tolerance in the north European *Crucian carp* and natural hypoxic preconditioning in a coral-reef shark. J. Exp. Biol. 207 (Pt 18), 3131–3139. https://doi.org/10.1242/jeb.00979.

Nilsson, G.E., Dymowska, A., Stecyk, J.A., 2012. New insights into the plasticity of gill structure. Respir. Physiol. Neurobiol. 184 (3), 214–222. https://doi.org/10.1016/j.resp.2012.07.012.

Qiang, J., Zhu, X.W., He, J., Tao, Y.F., Bao, J.W., Zhu, J.H., Xu, P., 2020. Mir-34a regulates the activity of hif-1a and p53 signalling pathways by promoting glut1 in genetically improved farmed tilapia (GIFT, *Oreochromis niloticus*) under hypoxia stress. Front. Physiol. 11, 670. https://doi.org/10.3389/fphys.2020.00670.

Ren, L., Li, W., Qin, Q., Dai, H., Han, F., Xiao, J., Gao, X., Cui, J., Wu, C., Yan, X., Wang, G., Liu, G., Liu, J., Li, J., Wan, Z., Yang, C., Zhang, C., Tao, M., Wang, J., Luo, K., Wang, S., Hu, F., Zhao, R., Li, X., Liu, M., Zheng, H., Zhou, R., Shu, Y., Wang, Y., Liu, Q., Tang, C., Duan, W., Liu, S., 2019. The subgenomes show asymmetric expression of alleles in hybrid lineages of *Megalobrama amblycephala* × *Culter alburnus*. Genome Res. 29 (11), 1805–1815. https://doi.org/10.1101/gr.249805.119.

Roesner, A., Mitz, S.A., Hankeln, T., Burmester, T., 2008. Globins and hypoxia adaptation in the goldfish, *Carassius auratus*. FEBS J. 275 (14), 3633–3643. https://doi.org/10.1111/j.1742-4658. 2008.06508.x.

Saddam, M., Paul, S.K., Habib, M.A., Fahim, M.A., Mimi, A., Islam, S., Paul, B., Helal, M. M.U., 2024. Emerging biomarkers and potential therapeutics of the bcl-2 protein family: the apoptotic and anti-apoptotic context. Egypt. J. Med. Human 25 (1). https://doi.org/10.1186/s43042-024-00485-7.

Sales, C.F., dos Santos, K.P.E., Rizzo, E., Ribeiro, R., dos Santos, H.B., Thomé, R.G., 2017. Proliferation, survival and cell death in fish gills remodeling: from injury to recovery. Fish Shellfish Immunol. 68, 10–18. https://doi.org/10.1016/j.fsi.2017.07.001.

Semenza, G.L., 2010. Hif-1: upstream and downstream of cancer metabolism. Curr. Opin. Genet. Dev. 20 (1), 51–56. https://doi.org/10.1016/j.gde.2009.10.009.

Shuang, L., Su, X.L., Zheng, G.D., Zou, S.M., 2022. Effects of hypoxia and reoxygenation on gill remodeling, apoptosis, and oxidative stress in hypoxia-tolerant new variety blunt snout bream (*Megalobrama amblycephala*). Fish Physiol. Biochem. 48 (1), 263–274. https://doi.org/10.1007/s10695-022-01047-7.

Sollid, J., De Angelis, P., Gundersen, K., Nilsson, G.E., 2003. Hypoxia induces adaptive and reversible gross morphological changes in *Crucian carp* gills. J. Exp. Biol. 206 (Pt 20), 3667–3673. https://doi.org/10.1242/jeb.00594.

Stecyk, J.A., Stenslokken, K.O., Farrell, A.P., Nilsson, G.E., 2004. Maintained cardiac pumping in anoxic *Crucian carp*. Science 306 (5693), 77. https://doi.org/10.1126/science.1100763.

Suo, N., Zhou, Z.X., Xu, J., Cao, D.C., Wu, B.Y., Zhang, H.Y., Xu, P., Zhao, Z.X., 2022. Transcriptome analysis reveals molecular underpinnings of common carp (*Cyprinus carpio*) under hypoxia stress. Front. Genet. 13. https://doi.org/10.3389/fgene.2022.907944.

Tao, Y.F., Qiang, J., Dagoudo, M., Zhu, H.J., Bao, J.W., Ma, J.L., Li, M.X., Xu, P., 2021. Transcriptome profiling reveals differential expression of immune-related genes in gills of hybrid yellow catfish (*Tachysurus fulvidraco* ♀ × *Pseudobagrus vachellii* ♂) under hypoxic stress: potential nlr-mediated immune response. Fish Shellfish Immunol. 119, 409–419. https://doi.org/10.1016/j.fsi.2021.10.023.

Tao, Y.F., Hua, J.X., Lu, S.Q., Wang, Q.C., Li, Y., Jiang, B.J., Dong, Y.L., Qiang, J., Xu, P., 2024. Ultrastructural, antioxidant, and metabolic responses of male genetically improved farmed Tilapia (GIFT, *Oreochromis niloticus*) to acute hypoxia stress. Antioxidants 13 (1). https://doi.org/10.3390/antiox13010089.

Wang, J., Chen, X., Ge, X., Wang, Z., Mu, W., 2022. Molecular cloning, characterization and expression analysis of p53 from high latitude fish *Phoxinus lagowskii* and its response to hypoxia. Fish Physiol. Biochem. 48 (3), 631–644. https://doi.org/10.1007/s10695-022-01072-6.

Wang, H.L., Guo, M., Wei, H.D., Chen, Y.H., 2023. Targeting p53 pathways: mechanisms, structures, and advances in therapy. Signal Transduct. Tar 8 (1). https://doi.org/10.1038/s41392-023-01347-1.

Weidemann, A., Johnson, R.S., 2008. Biology of hif-1alpha. Cell Death Differ. 15 (4), 621–627. https://doi.org/10.1038/cdd.2008.12.

Wen, X.M., Jiao, L.D., Tan, H., 2022. Mapk/erk pathway as a central regulator in vertebrate organ regeneration. Int. J. Mol. Sci. 23 (3). https://doi.org/10.3390/ijms23031464.

Wen, M., Zhu, C., Tang, Y., Zhang, H., Liu, Z., Wang, S., Tao, M., Hu, L., Rao, W., Li, S., Gong, D., Wang, S., Liu, S., 2025. Mechanism of hypoxia tolerance improvement in hybrid fish hefang bream. Aquaculture 599. https://doi.org/10.1016/j.aquaculture.2025.742199.

Wu, R.S.S., 2002. Hypoxia: from molecular responses to ecosystem responses. Mar. Pollut. Bull. 45 (1−12), 35–45. https://doi.org/10.1016/S0025-326X(02)00061-9.

Wu, C.B., Zheng, G.D., Zhao, X.Y., Zhou, S., Zou, S.M., 2020. Hypoxia tolerance in a selectively bred F 4 population of blunt snout bream (*Megalobrama amblycephala*) under hypoxic stress. Aquaculture 518, 734484. https://doi.org/10.1016/j.aquaculture.2019.734484.

Xiao, W., 2015. The hypoxia signalling pathway and hypoxic adaptation in fishes. Sci. China Life Sci. 58 (2), 148–155. https://doi.org/10.1007/s11427-015-4801-z.

Xing, M.C., Rong, Z., Zhao, X., Gao, X.W., Hou, Z.G., Zhang, L.H., Khor, W., Xu, Y.H., Chen, L., Wu, C.B., 2025. Transcriptome analysis reveals hypoxic response key genes and modules as well as adaptive mechanism of *Crucian carp* (*Carassius auratus*) gill under hypoxic stress. Front. Immunol. 16. https://doi.org/10.3389/fimmu.2025.1543605.

Xu, X.N., Chen, S.L., Jiang, Z.X., Nissa, M.U., Zou, S.M., 2022. Gill remodeling increases the respiratory surface area of grass carp (*Ctenopharyngodon idella*) under hypoxic stress. Comp. Biochem. Physiol. A Mol. Integr. Physiol. 272. https://doi.org/10.1016/j.cbpa.2022.111278.

Yu, X.X., Zhang, Y.R., Li, S.S., Zheng, G.D., Zou, S.M., 2023. Effects of hypoxia on the gill morphological structure, apoptosis and hypoxia-related gene expression in blunt snout bream (*Megalobrama amblycephala*). Fish Physiol. Biochem. 49 (5), 939–949. https://doi.org/10.1007/s10695-023-01233-1.

Zhang, Y.X., Beachy, P.A., 2023. Cellular and molecular mechanisms of hedgehog signalling. Nat. Rev. Mol. Cell Biol. 24 (9), 668–687. https://doi.org/10.1038/s41580-023-00591-1.

Zhou, B.H., Lin, W.L., Long, Y.L., Yang, Y.K., Zhang, H., Wu, K.M., Chu, Q., 2022. Notch signalling pathway: architecture, disease, and therapeutics. Signal Transduct. Tar 7 (1). https://doi.org/10.1038/s41392-022-00934-y.

Zhu, C.D., Wang, Z.H., Yan, B., 2013. Strategies for hypoxia adaptation in fish species: a review. J. Comp. Physiol. B. 183 (8), 1005–1013. https://doi.org/10.1007/s00360-013-0762-3.

Zhu, T.T., Chen, R.F., Wang, J.Y., Yue, H.R., Lu, X., Li, J., 2020. The prognostic value of itga and itgb superfamily members in patients with high grade serous ovarian cancer. Cancer Cell Int. 20 (1). https://doi.org/10.1186/s12935-020-01344-2.